



The Torak granitic massif: structure, petrology, and mineralogy (Tefedest, Central Hoggar, Algeria)

Faiza Ikhlef-Debabha^{1,2} · Abla Azzouni-Sekkal^{2,3} · Amel-Zoulikha Benhalou^{1,2} · Delphine Bosch⁴ · Carlos Marin Garrido⁵ · Youcef Babkar^{1,6} · Zakaria Boukhalfa⁷ · Khaled Aghanbilou^{1,6}

Received: 6 August 2019 / Accepted: 1 July 2020 / Published online: 15 July 2020
© Saudi Society for Geosciences 2020

Abstract

The Torak massif located to the west of the Atakor volcanic district is a granitic pluton NNE-SSW elongated and crosscut by several NNW-SSE lineaments. It is intrusive within the S-W Tefedest terrane composed of Eburnean (c. 2 Ga) gneisses and of Pan-African (c. 615 Ma) syntectonic granitic batholiths. New field mapping, petrographic, and mineralogical data (feldspars and mica chemistry) and geochemical data (major and trace elements, REE) reveal the following: the Torak granitic massif shows a fairly simple and homogenous mineralogy dominated by feldspars (orthoclase and microcline, albite, and oligoclase) and lithium micas (siderophyllite to protolithionite and phengite to Li-phengite). The Torak granite chemistry is remarkably homogeneous both in major elements ($73.95 \leq \text{SiO}_2 \leq 76.85$ wt.%; $7.68 \leq (\text{Na}_2\text{O} + \text{K}_2\text{O}) \leq 9.55$ wt.%) and trace elements ($500 \leq \text{Rb} \leq 780$ ppm; $9.774 \leq \text{La} \leq 45.267$ ppm; $0.316 \leq (\text{La/Yb})_N \leq 2.418$; $0.027 \leq (\text{Eu/Eu}^*) \leq 0.064$). This data indicates that Torak rocks are highly fractionated calk-alkaline (HFCA) and co-genetic granites having evolved by assimilation-fractional crystallization (AFC). Similar to the surrounding GIIb granites of the Taourirt province (Azzouni-Sekkal & Boissonnas in Bulletin Société Géologique France 164: 597–608, 1993; Azzouni-Sekkal et al. in J Afr Earth Sci 37: 337–350, 2003), a similar mixed deep source (asthenosphere + old lower crust) can be described here. The country rocks could correspond to the old Archaean–Paleoproterozoic LATEA metacraton. The emplacement of the Torak pluton could be linked to the Murzukian intracontinental orogenic phase that occurred in the eastern part of the Tuareg Shield (Fezaa et al. in Precambrian Res 180: 299–327, 2010).

Keywords Torak · Alkali-calcic Taourirt · Granite · Post-collisional · LATEA · Hoggar · Lithic micas

Introduction

The Tuareg shield in North-West Africa is composed of an assembly of Neoproterozoic continental and oceanic terranes, as well as Archean and Paleoproterozoic terranes separated by major continental shear zones. It comprises Hoggar in Algeria,

Adrar des Iforas in Mali, and Aïr Mountains in Niger (Black et al. 1994). It is composed of 25 terranes juxtaposed after large displacements along mega-shear zones mostly N-S oriented (Black et al. 1994; Liégeois et al. 2003; Liégeois 2019) (Fig. 1a).

The “Taourirt” province represents the last plutons emplaced in central Hoggar at 539–523 Ma where three

Responsible Editor: Domenico M. Doronzo

✉ Faiza Ikhlef-Debabha
debabhaf@yahoo.fr

¹ Centre de recherche en astronomie, astrophysique et géophysique (CRAAG), route de l’Observatoire, BP 63, Bouzaréah, Algeria

² FSTGAT, USTHB, BP 32, El Alia, 16111 Bab Ezzouar, Algeria

³ Département des Sciences de la Terre Faculté des Sciences de la vie, de la Terre et de l’Univers Université Aboubekr Belkaïd, Tlemcen, BP 119, 13000 Tlemcen, Algeria

⁴ CNRS, Géosciences Montpellier - UMR 5243 CNRS - Univ. de Montpellier - Univ. des Antilles Observatoire des Sciences de l’Univers, OSU OReME, Place E. Bataillon, Bât. 22 - cc 060, 34095 Montpellier, cedex 05, France

⁵ Instituto Andaluz de Ciencias de la Tierra (IACT), CSIC & Universidad de Granada, Avenida de las Palmeras 4, 18100 Armilla, Granada, Spain

⁶ Observatory of Tamanrasset, CRAAG, BP 32, El hofra, Tamanrasset, Algeria

⁷ School of Earth Sciences, Zhejiang University, 38 Zheda Road, Hangzhou 210008, Zhejiang Province, China

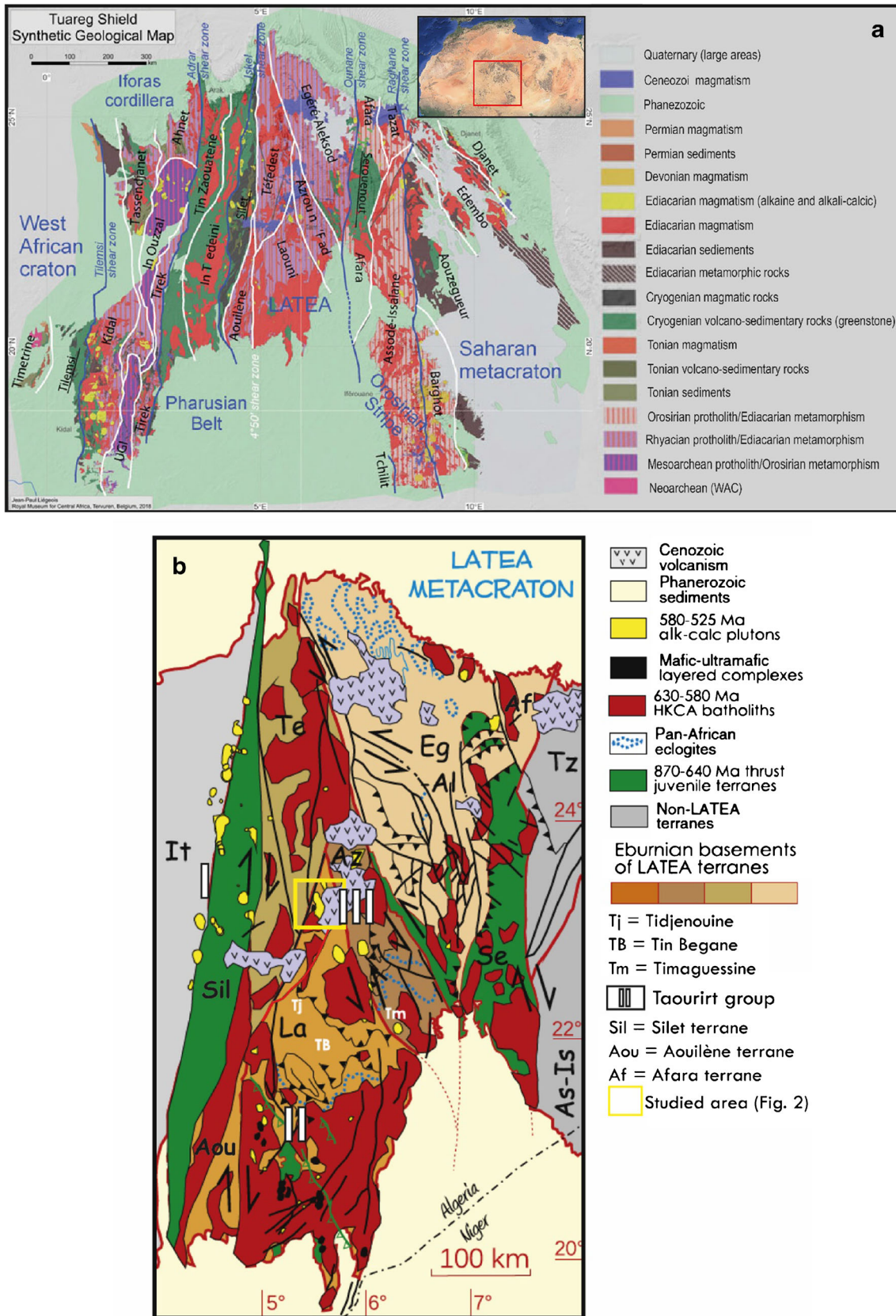


Fig. 1 **a** Synthetic geological map of the Tuareg Shield with the delimitation of the 25 terranes (separated by white or blue lines). Two terranes have been added (Aouilène and Afara) to those of Black et al. (1994). **b** Geological map of the LATEA metacraton showing the preserved Archean Paleoproterozoic basement (metacraton) dissected in five terranes (La = Laouni, Az = Azrou-n-Fad, Te = Tefedest, Eg-Al = Egéré-Aleksod and Aou = Aouilène), the thrust juvenile Cryogenian terranes (Sil = Silet Se = Serouenout with additional more localized material such as the eclogitic bands), the high-K calc-alkaline (HKCA) batholiths (630–580 Ma), the mantle-derived mafic-ultramafic layered complexes, the alkaline/alkali-calcic plutons (principally Taourirt Province) and the Cenozoic Tuareg volcanism mainly located in the LATEA metacraton. Neighbor terranes are In Tedeini (It), Tazat (Tz), and Assodé Issalane (As-Is). With the three proposed Taourirt groups: I: Silet-Taourirt; II: Laouni-Taourirt; III: Tamanrasset-Taourirt. Adapted from Azzouni et al. (2003), Liégeois et al. (2013) and Liégeois (2019)

geographical groups were identified (Azzouni-Sekkal et al. 2003): the Silet-, Laouni-, and Tamanrasset-Taourirt. The proposed model for the genesis of the Taourirt province is the last movements along the mega-shear zones that dissected the LATEA metacraton (LATEA is the acronym of the terranes constituting this metacraton: Laouni–Azrou-n-Fad–Tefedest–Egéré–Aleksod–Aouilène; metacraton is a notion proposed by Abdelsalam et al. (2002) defined as a craton that has been remobilized during an orogenic event but that is still recognized dominantly through its rheological, geochronological, and isotopic characteristics (Liégeois et al. 2003; Liégeois 2019), provoked linear delamination, and asthenosphere uprise, and lead to a mixed asthenospheric/old lower crust source (Azzouni-Sekkal et al. 2003, Fezaa et al. 2010).

The Torak pluton outcrops in the Tefedest terrane (LATEA metacraton). Torak constitutes the south part of the Taessa massif (Boissonnas 1974) and belongs to the Tamanrasset Tourirt group (Fig. 1b). It has been almost not studied, except for the petrographic observations (Boissonnas 1974). Indeed, a number of felsic volcanic highs and basaltic plateaus of the Atakor district govern landscape and make access to the area almost impossible.

Modern geological study is presented in this paper. This study combines field observations, petrography, mineralogy, and geochemistry (major, trace elements, and REE), of the Torak rocks. Its aims are (i) draw a new map using remote sensing and various digital processing methods, such as color processing, band ratios, etc....; (ii) to debate the relation with the surrounding Taourit granites of the LATEA; (iii) to detect igneous differentiation mechanisms leading to high-evolved compositions and to discuss origin and possible contamination of the magmas.

Geological setting

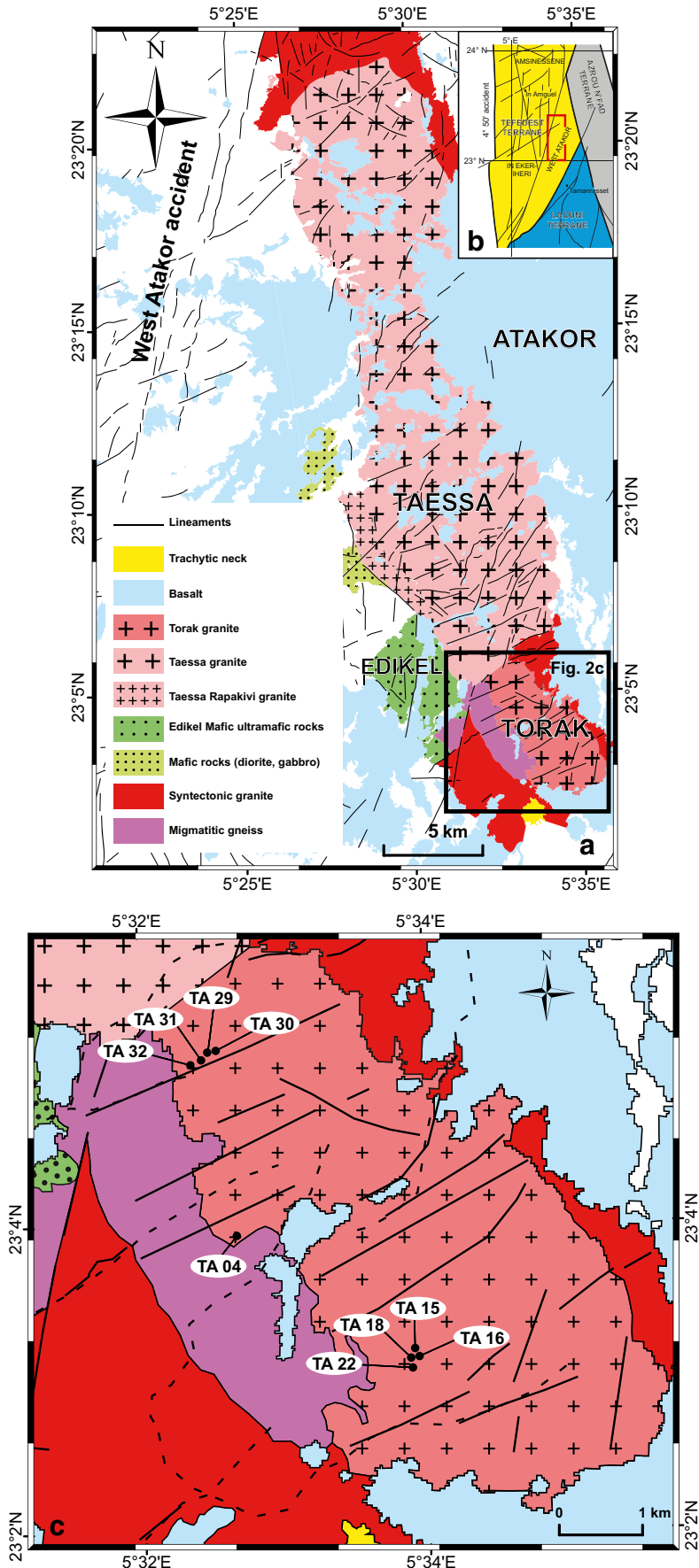
LATEA metacraton (Fig. 1b) is located in the central part of the shield (Central Hoggar); it is composed of well-preserved amphibolite to granulite-facies Archean and

Paleoproterozoic terranes despite the major Panafrican reworking (Liégeois et al. 2003; Peucat et al. 2003; Bendaoud et al. 2008). Mega-shear zones and intrusion of batholiths (Bertrand et al. 1978; Acef et al. 2003) (Fig. 1b) mark the metacratonization of LATEA (metacratonization process occurred when the LATEA craton was squeezed between the nearly opposite pushing of the West African Craton WAC and the Saharan metacraton SmC. This squeezing generated a general tectonic escape to the north of the Tuareg shield terranes. LATEA was not able to behave as one rigid body. It was dissected by mega-shear zones and intruded by HKCA batholiths and finally by shallow depth alkaline plutons; Liégeois et al. 2003). This event is accompanied by (H-T) amphibolitic facies metamorphism (Bendaoud et al. 2008) occurred mainly at 620–600 Ma (Bertrand et al. 1978; Acef et al. 2003; Bendaoud et al. 2008). This H-T stage ended at c. 572 Ma, when high-level sub-circular plutons such as the Temaguessine pluton intruded (Abdallah et al. 2007) followed by alkaline-peralkaline complexes (Azzouni et al., work in progress). Later, and probably in consequence of the 575–545 Ma intra-cratonic Murzukian event (Fezaa et al. 2010; Liégeois et al. 2013) with only brittle limited reactivations of some shear zones within the LATEA metacraton, sub-circular alkali-calcic complexes called “Taourirt” suite (535–525 Ma) (Boissonnas 1974; Azzouni-Sekkal et al. 2003) intruded the basement, (Fig. 1b). Some are granites mineralized with albite-topaz (Cheilletz et al. 1992; Ahmed-Said et al. 1995; Chalal and Marignac 1997; Kesraoui and Nedjari 2002) and constitute the most evolved terms of the Taourirt suite, which set up on the boundary between the block of Laouni and Azrou-n-Fad.

The field study, named “The West Atakor domain” by Vitel (1979) (Fig. 2a), is limited to the West by the great West-Atakor dislocation oriented N 20° flanked by mylonitized rocks of kilometric thickness. The formations of this group are mostly hidden under the basaltic traps of the Atakor and the Manzaz massifs. The eastern limit is constituted by a large fault of Irharhar Oued, NNW-SSE. This fault separates the group from that of Tamanrasset further south, lithologically and structurally different. In this area, the magmatic rocks are dominant and consist of a succession of Neoproterozoic acid and basic igneous rocks and Cenozoic volcanism (Fig. 2a, b).

Torak pluton outcrops 30 km north of Tamanrasset between 23° 2' and 23° 6' latitudes and 5° 31' and 5° 36' longitudes (Fig. 2c). Torak is a small unit 7.5 km long oriented NNW-SSE and constitutes the southern part of Taessa granitic massif (Fig. 2a). In the west, Torak outcrops in the Eburnean migmatitic gneisses and granites and adjoins the ultramafic Edikel massif (Ikhlef-Debabha et al. 2014) (Fig. 3a). To the east, it crosscuts the early syntectonic Atakor granites (Fig. 3b). It is partially covered by Atakor lava towards the southern and eastern parts (Fig. 2c). A convex limit towards the Taessa

Fig. 2 **a** Geological Map of the West Atakor domain, Hoggar, Algeria (Using Landsat 7 ETM+ for lithological and structural mapping) adapted from Ikhlef-Debabha et al. (2014). **b** Geological map of the Tafedest terrane components (Adapted from Vitel 1979). **c** Enlarged geological map of the Torak pluton with sample locations. Legend of symbols given in Fig. 2a



stricto sensu appears on the aerial photography and even on the Google Earth satellite image but it remains difficult to find and follow on the field. On the roof of this formation, that is to say the contact, Boissonnas (1974) observed webbed microclines (the webbed structure is a mineral structure, which appears when the mineral ramifications are very close to each other and then present a palm shape) whose points are directed towards Taessa. The Torak massif therefore seems a little more recent than the Taessa granites but nothing indicates a big hiatus in time. The absence of geometrical criteria (angular enclaves of one granite in the other, parallel-edges veins ...) leads us to admit that the two sets are partly synchronous. Simply, the Torak would have crystallized after the rest of the complex (Boissonnas 1974).

Torak is composed of coarse porphyritic granites, sometimes showing alignment of feldspars (Fig. 3d), and medium to fine-grained pink granites. To the south, greisens have

formed at the expense of the porphyritic granite, and are enclosed in the intrusive mass. To the north, we observe some nests of micas, almost metric pegmatite and quartz veins highlighting contact with the Taessa massif (Fig. 3 c and e).

Field observations, aerial photographs, and Landsat ETM 7 imagery allowed local-scale discrimination of geological units including the different generations of granites (Fig. 2a). This was made through a combination of various digital processing methods, such as color processing and band ratios (5/3, 4/2, 3/1) and (5/7, 3/1, 4/3) (Fig. 4a, b). The use of directional filters (3×3 matrices) at 135° , 45° , and 00° , made possible to establish precise cartography of lineaments occurring in the studied area (Fig. 4c). The highest concentration of lineaments occurs in the northern and southern parts of the studied area. Two predominant directions emerge. The sub-meridian directions (NNE-SSW) to meridian are the most important: they represent the dextral strike of the West Atakor fault (Fig. 4d).

Fig. 3 Field pictures: **a** View of the different geologic units of the studied area (West Atakor domain). **b** Contact between the Torak granite and migmatitic gneiss. **c** Coarse-grained porphyritic granite. **d** Medium to fine-grained alkaline granite. **e** Metric quartz vein within Torak granite

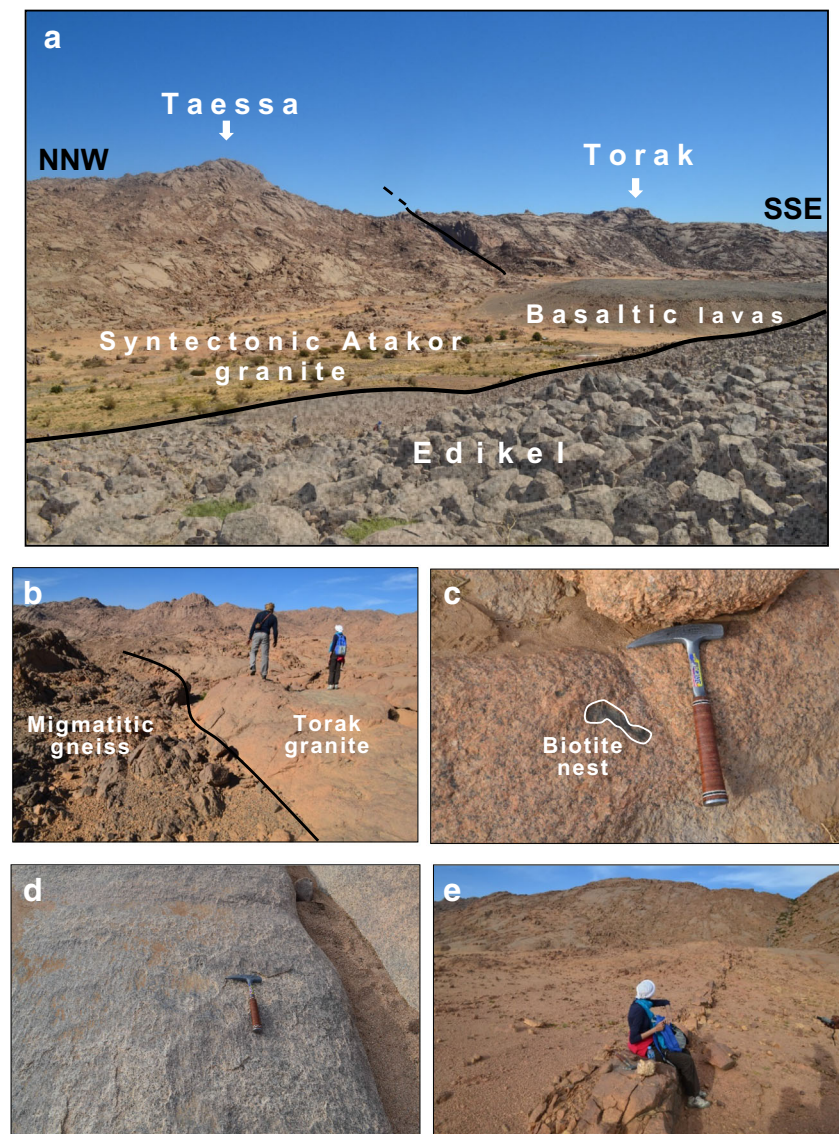
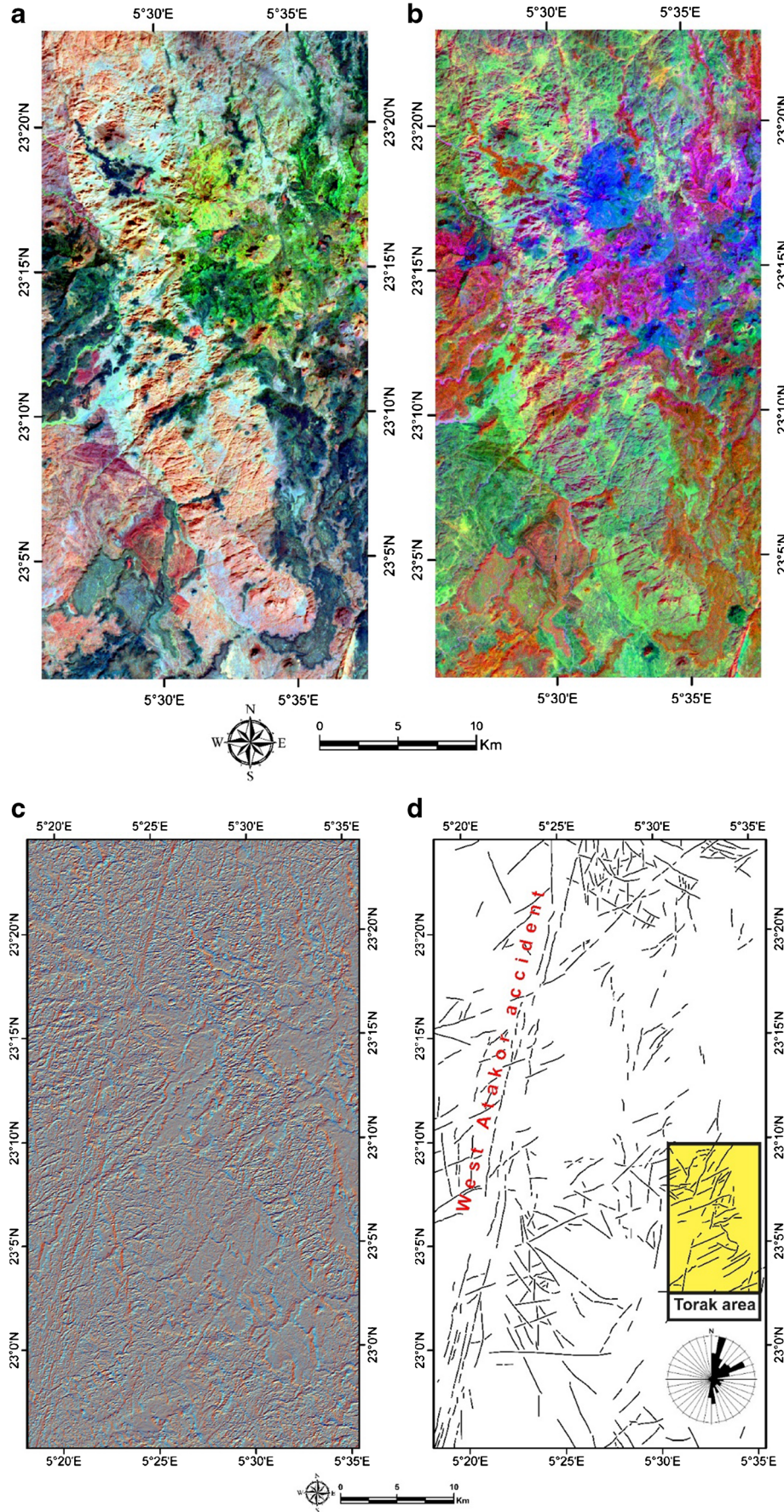


Fig. 4 Landsat 7 ETM scene extract in different color composites showing the distinction between the different geological units of the studied area. **a** band ratios (5/3, 4/2, 3/1). **b** band ratios (5/7, 3/1, 4/3). **c** Landsat 7 ETM scene extract from directional filters (3×3 matrices) at 135° , 45° and 00° of the west Atakor domain. **d** Lineaments map derived from satellites images of the west Atakor domain and rose diagram showing the distribution of the lineaments directions



ENE-WSW ($61\text{--}70^\circ$) directions subparallel to each other intersect the Torak massif and the extreme south of the Taessa massif stricto sensu (Fig. 4d); they are underlined by late quartz and aplite dykes and veins.

Petrography

The Torak pluton is composed of five main types of granitoids, showing a fairly simple and homogenous mineralogy; two-mica granite, biotite granite, alaskite, alkaline granite, and greisen:

Two-mica granite (Fig. 5a) occurs in the southern part of Torak. These granites are coarse to medium grained. They show abundant K-feldspar mega-crysts that give a pinkish color to the rocks, well-developed quartz of 8 mm on average, and dark mica appears in irregularly sparse black spots (up to 2 mm), as well as some white mica with silvery luster (1 mm on average). The K-feldspar is represented by orthoclase and microcline (up to 5 mm), quartz occurs as large xenomorphic crystals and plagioclase forms automorphic tabular crystals (up to 2 mm). Xenomorphic biotite flakes, partially altered by chlorite, contain zircon (0.04 mm on average). Heterogranular white mica locally shows purplish-yellow pleochroism. Zircon has elongated, rounded, or square form,

Fig. 5 Microfabric of the different Torak facies. **a** Two-mica granite; **b** Biotite and zircon in biotite granite; **c** Fluorite in biotite granite. **d** Monazite in biotite granite. **e** Microcline and orthoclase in alaskite. **f** Texture of alaskite. **g** Texture of alkali-granite. **h** Allanite in greisen (Fl: fluorite; All: allanite; Qz: quartz; Or: orthoclase; Bt: biotite; Ms: muscovite; Mc: microcline; Mo: monazite; Zr: zircon)

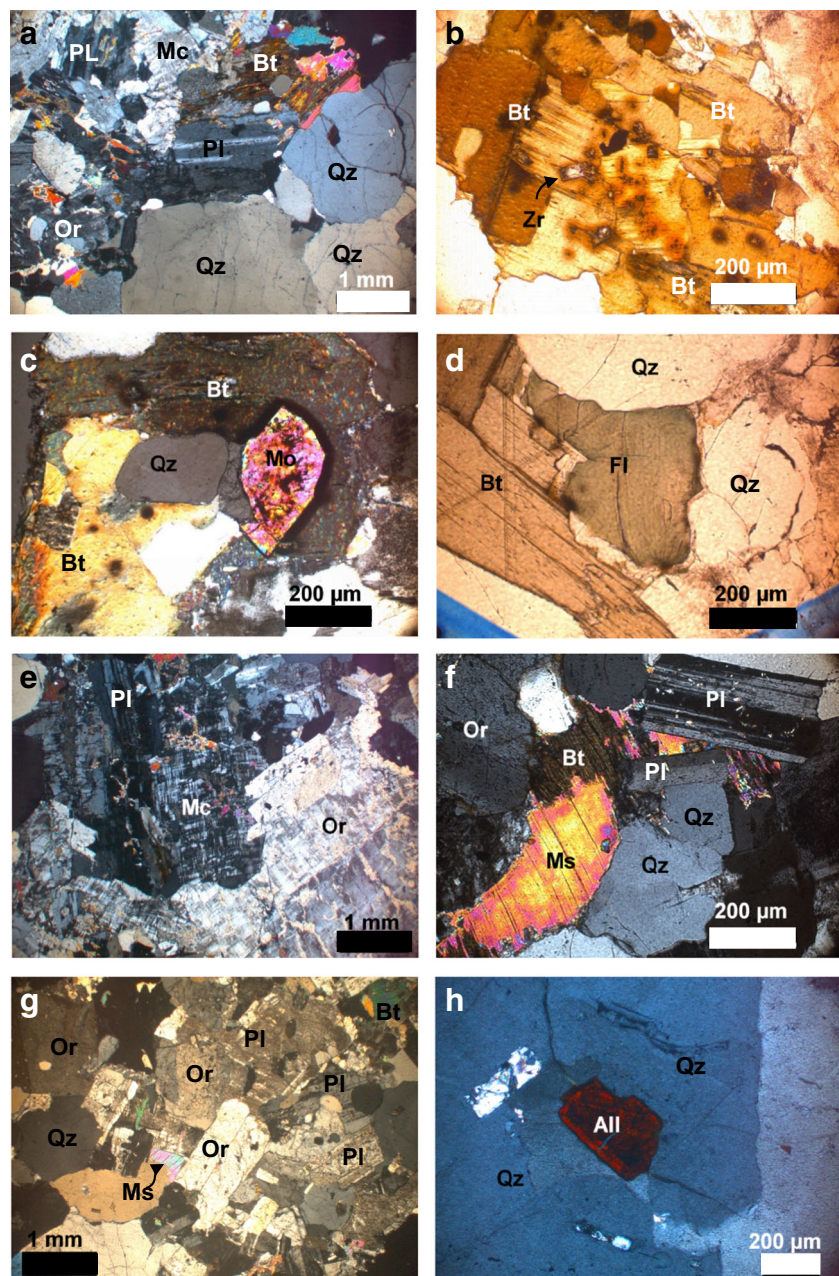


Table 1 Selected electron-microprobe analyses of feldspars (analyze in wt%) from Torak granitoids

Facies	Two-mica granite							Biotite granite										
	Sample				Ta 18			Ta 15			TA 29							
Analyze N°																		
SiO ₂	68.21	67.57	63.97	67.59	67.22	63.32	67.57	68.15	69.63	69.59	66.98	69.67	65.70	68.09	65.88	65.82		
TiO ₂	0.00	0.00	0.00	0.00	0.00	0.00	0.01	0.00	0.03	0.00	0.00	0.00	0.01	0.00	0.02	0.02		
Al ₂ O ₃	19.74	19.75	18.43	20.08	19.92	18.23	21.16	20.47	19.42	20.01	21.31	19.73	18.24	20.82	18.33	18.53		
FeO*	0.00	0.01	0.13	0.02	0.02	0.00	0.00	0.02	0.02	0.00	0.01	0.00	0.03	0.02	0.04	0.03		
MnO	0.00	0.01	0.01	0.00	0.00	0.00	0.00	0.01	0.00	0.00	0.00	0.00	0.00	0.00	0.01	0.01		
MgO	0.00	0.00	0.00	0.00	0.00	0.00	0.01	0.00	0.00	0.02	0.01	0.00	0.02	0.00	0.01	0.00		
CaO	0.11	0.35	0.00	0.63	0.45	0.00	2.13	1.49	0.34	0.61	2.36	0.24	0.00	1.73	0.02	0.01		
Na ₂ O	11.08	10.82	0.21	11.01	10.51	0.28	10.11	10.62	11.05	11.31	10.17	11.37	0.50	10.21	0.43	0.68		
K ₂ O	0.14	0.13	17.40	0.07	0.13	17.35	0.26	0.13	0.20	0.07	0.17	0.24	17.19	0.20	17.21	16.82		
Total	99.28	98.64	100.15	99.40	98.25	99.19	101.26	100.88	100.69	101.61	101.01	101.25	101.69	101.06	101.95	101.92		
Number of ions (on basis of 32 oxygen)																		
Si	2.994	2.986	2.976	2.969	2.980	2.976	2.924	2.955	3.013	2.989	2.910	3.002	3.000	2.946	3.000	2.994		
Al	1.021	1.029	1.011	1.040	1.041	1.010	1.080	1.046	0.991	1.013	1.091	1.002	0.982	1.062	0.984	0.993		
Ca	0.005	0.017	0.000	0.030	0.021	0.000	0.099	0.069	0.016	0.028	0.110	0.011	0.000	0.080	0.001	0.001		
Na	0.943	0.927	0.019	0.938	0.903	0.026	0.848	0.893	0.927	0.942	0.857	0.950	0.044	0.856	0.038	0.060		
K	0.008	0.007	1.033	0.004	0.007	1.040	0.014	0.007	0.011	0.004	0.009	0.013	1.002	0.011	1.000	0.976		
Sum cations	4.971	4.966	5.038	4.981	4.954	5.052	4.965	4.971	4.958	4.976	4.976	4.978	5.028	4.956	5.023	5.024		
An	0.533	1.758	0.000	3.050	2.285	0.000	10.277	7.136	1.646	2.881	11.240	1.127	0.022	8.446	0.070	0.049		
Ab	98.627	97.471	1.779	96.537	96.942	2.399	88.257	92.123	97.172	96.698	87.812	97.540	4.195	90.384	3.657	5.806		
Or	0.840	0.770	98.221	0.413	0.773	97.601	1.466	0.741	1.182	0.421	0.949	1.333	95.783	1.170	96.273	94.146		
Facies																		
Biotite granite																		
Sample																		
TA 04					TA 30							Alaskite						
Analyze N°	9c	12c	13c	14c	52r	54c	55c	32c	33r	34r	35c	5c	16c	17r	18r			
SiO ₂	69.25	64.15	67.92	67.27	69.30	66.25	65.83	68.97	69.42	68.72	68.81	69.49	69.64	69.66	70.15			
TiO ₂	0.01	0.03	0.00	0.00	0.01	0.01	0.00	0.00	0.00	0.02	0.01	0.00	0.02	0.02	0.02			
Al ₂ O ₃	19.39	18.12	19.47	19.97	19.80	18.41	18.31	19.37	19.46	19.41	19.71	19.40	19.47	19.32	19.52			
FeO*	0.01	0.02	0.02	0.01	0.01	0.03	0.03	0.03	0.01	0.01	0.01	0.01	0.01	0.03	0.03			
MnO	0.00	0.00	0.00	0.01	0.00	0.00	0.00	0.00	0.00	0.00	0.00	0.01	0.01	0.00	0.00			
MgO	0.00	0.02	0.00	0.01	0.00	0.01	0.00	0.00	0.00	0.00	0.00	0.00	0.01	0.00	0.00			
CaO	0.02	0.00	0.38	0.69	0.58	0.01	0.04	0.04	0.03	0.16	0.22	0.14	0.10	0.09	0.13			
Na ₂ O	11.10	0.36	10.64	10.45	11.13	1.29	1.04	10.80	10.97	10.68	10.85	11.42	11.55	11.90	11.32			
K ₂ O	0.07	17.14	0.19	0.23	0.09	15.83	16.29	0.08	0.07	0.24	0.15	0.19	0.22	0.13	0.16			
TOTAL	99.85	99.86	98.63	98.66	100.92	101.84	101.53	99.30	99.98	99.24	99.77	100.67	101.03	101.14	101.32			
Number of ions (on basis of 32 oxygen)																		
Si	3.017	2.988	2.999	2.975	2.995	3.003	3.001	3.018	3.018	3.013	3.002	3.011	3.008	3.008	3.016			
Al	0.996	0.995	1.014	1.041	1.009	0.984	0.984	1.000	0.998	1.003	1.014	0.991	0.992	0.983	0.989			
Ca	0.001	0.000	0.018	0.033	0.027	0.001	0.002	0.002	0.002	0.008	0.010	0.007	0.005	0.004	0.006			
Na	0.937	0.033	0.911	0.896	0.932	0.113	0.092	0.917	0.925	0.908	0.918	0.959	0.967	0.997	0.943			
K	0.004	1.019	0.011	0.013	0.005	0.915	0.948	0.004	0.004	0.013	0.008	0.011	0.012	0.007	0.009			
Sum cations	4.955	5.035	4.954	4.958	4.968	5.016	5.026	4.941	4.947	4.945	4.952	4.978	4.984	5.000	4.963			
An	0.103	0.004	1.929	3.458	2.800	0.066	0.173	0.204	0.164	0.814	1.113	0.687	0.483	0.420	0.609			
Ab	99.508	3.104	96.924	95.147	96.682	11.002	8.795	99.314	99.402	97.742	97.993	98.221	98.293	98.890	98.447			
Or	0.389	96.892	1.147	1.395	0.518	88.932	91.033	0.483	0.433	1.443	0.893	1.092	1.223	0.689	0.944			

*Total iron as FeO. An, anorthite; Ab, albite; Or, orthoite; c, core; r, rim

generally found as inclusion in biotite, and in lesser importance in quartz and feldspar. Monazite and xenotime with brown and very large pleochroic aureoles are included in biotite, which also occur around zircon. Locally, apatite is found in quartz. Flakes of secondary muscovite develop on the feldspars.

The biotite granite presents the same characteristics as the two-mica granite, having in addition opaque oxides and widespread zircon and monazite (up to 0.25 mm) (Fig. 5b, c), only occasionally fluorites (up to 0.3 mm) (Fig. 5d), and no primary muscovite.

Alaskites (Fig. 5e, f) occurring in the northern part of Torak is leucocratic granite with equigranular fine-grained texture. Quartz crystals are rounded; feldspars are pink to white irregularly arranged. The dark-colored minerals are grouped into small-scattered clusters, giving the rock a speckled appearance. Quartz (up to 0.7 mm) is highly abundant in large xenomorphic crystals with undulose extinction. It contains rare and small zircons or in sub-automorphic grains. The dominant K-feldspar is microcline with wide sub-square crystals (up to 0.7 mm); orthoclase and perthitic orthoclase (up to 0.5 mm) are also present. Plagioclase (up to 0.4 mm) is small compared to K-feldspar in sub-automorphic tabular crystals

with several inclusions as biotite, quartz, zircon, and secondary muscovite. Biotite is scarce in isolated and elongated flakes or in clusters (up to 0.2 mm). It is locally chloritized and associated with opaque minerals. Heterogranular muscovite is in accessory modal amounts and is irregularly distributed (0.1 on average). The secondary minerals are fluorite (up to 0.07 mm) characterized by a greenish color and chlorite.

Small prismatic or rounded zircon (up to 0.04 mm) is included in biotite, or locally forms clusters in quartz. Opaque oxides are xenomorphic and well developed (up to 0.2 mm) associated with quartz and feldspar.

Alkaline granite (Fig. 5g) occurs in the South Torak massif. It is a medium-grained pink granite composed of quartz, alkaline feldspars, and albite. Quartz is abundant (2 mm on

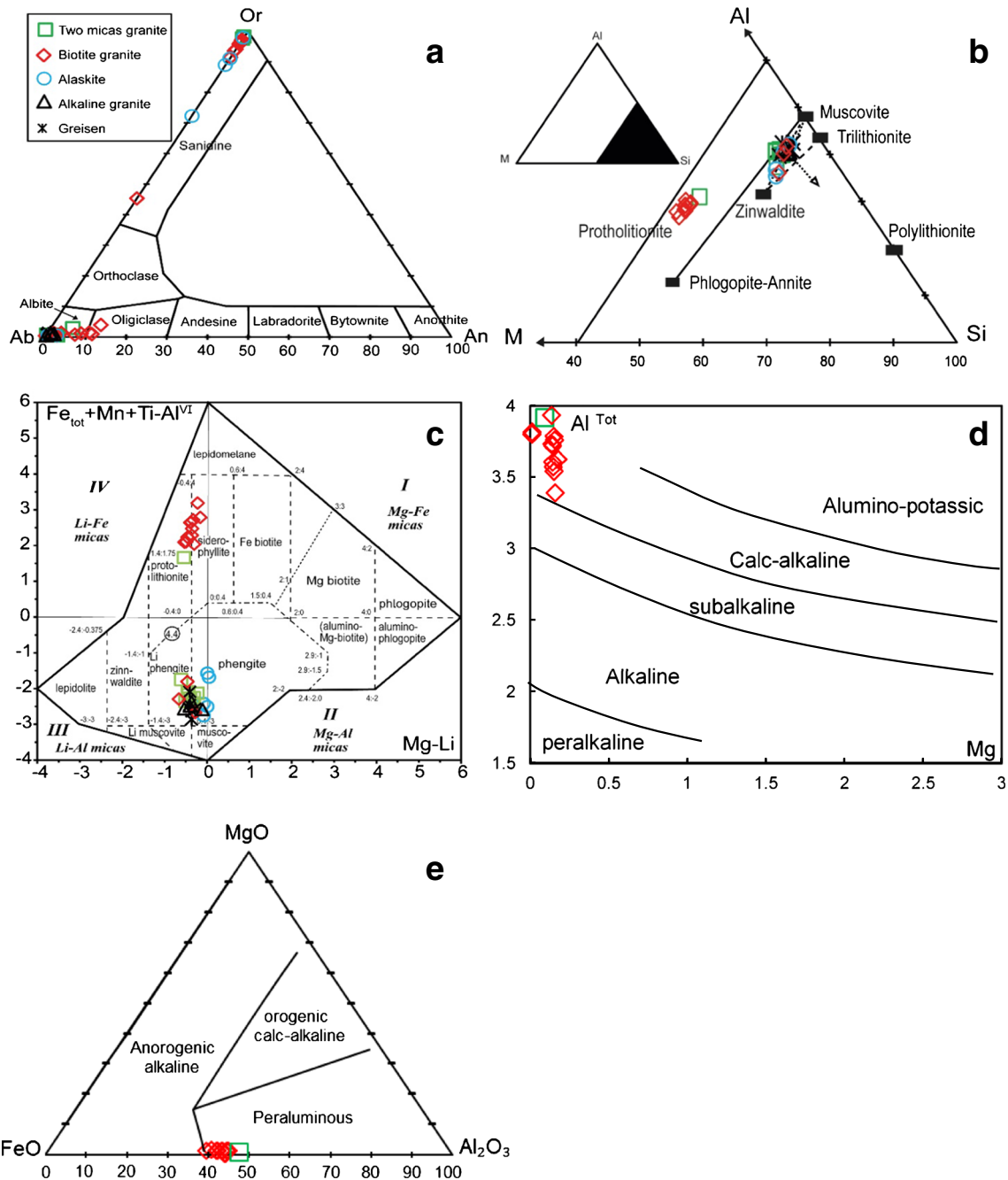


Fig. 6 Mineral chemistry from the different granite facies of the Torak massif. **a** Feldspars in the Or-Ab-An diagram. **b** Mica compositions reported in the $\text{M}^{2+} = (\text{Fe} + \text{Mn} + \text{Mg}) - \text{Al} - \text{Si}$ diagram (Monier 1987). **c** Mica compositions reported in the $\text{mgl} = \text{Mg} - \text{Li}$ and $\text{feal} = \text{Fe} + \text{Mn} +$

$\text{Ti} - \text{Al}^{\text{VI}}$ diagram (Tischendorf et al. 1997, 1999). **d** Biotite plotted in the Al^{tot} versus Mg diagram (Nachit et al. 1966). **e** Biotite plotted in the wt.% $\text{FeO}-\text{MgO}-\text{Al}_2\text{O}_3$ diagram (Abdel-Rahman 1994)

Table 2 Selected electron-microprobe analyses of trioctahedral micas (analyze in wt%) from Torak granitoids

Facies	Two-mica granite	Biotite granite										
Sample	TA 15	TA 29	TA 04									
N° analyze	23	20	21	23	26	27	33	44	45	46	4 c	5 r
SiO ₂	37.00	37.34	36.20	36.10	35.51	36.27	35.85	36.47	36.33	36.79	36.37	36.36
TiO ₂	1.03	1.06	1.77	2.49	3.02	0.89	0.31	2.11	2.13	1.60	0.67	0.52
Al ₂ O ₃	21.71	21.36	20.64	19.47	18.42	20.68	21.44	19.80	19.99	20.80	20.86	20.68
FeO*	24.12	26.33	27.10	26.93	28.29	26.88	26.40	27.26	27.40	26.10	26.27	26.31
MnO	0.30	0.54	0.53	0.54	0.59	0.56	0.60	0.53	0.53	0.53	0.65	0.64
MgO	0.41	0.68	0.63	0.66	0.68	0.68	0.58	0.64	0.63	0.61	0.19	0.15
CaO	0.00	0.00	0.01	0.00	0.00	0.01	0.00	0.00	0.00	0.00	0.04	0.00
Na ₂ O	0.07	0.11	0.13	0.09	0.09	0.09	0.14	0.05	0.10	0.10	0.13	0.09
K ₂ O	10.37	9.88	10.03	10.18	9.83	9.97	9.81	10.24	9.98	10.12	10.06	9.96
Li ₂ O	1.04	1.13	0.80	0.78	0.60	0.83	0.70	0.88	0.84	0.98	0.85	0.85
F	2.82	1.67	1.52	1.45	0.87	1.95	1.72	1.44	1.20	1.68	2.36	2.66
Total	98.93	100.11	99.36	98.68	97.91	98.81	97.56	99.43	99.13	99.30	98.44	98.22
Number of ions (on basis of 22 oxygens)												
Si	5.663	5.618	5.540	5.575	5.545	5.599	5.580	5.584	5.564	5.604	5.646	5.674
Al ^{IV}	2.337	2.382	2.460	2.425	2.455	2.401	2.420	2.416	2.436	2.396	2.354	2.326
Al ^{VI}	1.580	1.406	1.263	1.118	0.936	1.361	1.514	1.158	1.171	1.338	1.463	1.478
Ti	0.119	0.120	0.204	0.289	0.354	0.104	0.036	0.243	0.245	0.183	0.078	0.061
Fe	3.087	3.313	3.468	3.478	3.694	3.470	3.436	3.491	3.509	3.324	3.410	3.434
Mn	0.039	0.069	0.069	0.070	0.078	0.073	0.079	0.069	0.069	0.068	0.085	0.085
Mg	0.093	0.151	0.143	0.153	0.159	0.155	0.135	0.147	0.143	0.137	0.043	0.034
Li	0.638	0.686	0.495	0.482	0.380	0.512	0.441	0.544	0.518	0.598	0.533	0.533
Ca	0.000	0.000	0.001	0.000	0.000	0.001	0.000	0.000	0.001	0.000	0.006	0.000
Na	0.020	0.033	0.039	0.028	0.028	0.027	0.041	0.016	0.030	0.029	0.038	0.027
K	2.026	1.897	1.958	2.006	1.959	1.964	1.948	1.999	1.951	1.967	1.992	1.984
F	1.364	0.797	0.738	0.707	0.431	0.953	0.844	0.697	1.364	0.811	1.157	1.313
OH	2.621	3.203	3.262	3.293	3.569	3.047	3.156	3.303	2.621	3.189	2.843	2.687
sum cations	15.601	15.676	15.641	15.622	15.588	15.668	15.631	15.666	15.637	15.643	15.649	15.635
Fe/Fe + Mg	0.971	0.956	0.960	0.958	0.959	0.957	0.962	0.960	0.961	0.960	0.987	0.990
mgli	-0.545	-0.534	-0.352	-0.329	-0.221	-0.357	-0.305	-0.397	-0.375	-0.460	-0.490	-0.499
feal	1.664	2.096	2.478	2.719	3.190	2.286	2.038	2.644	2.652	2.236	2.110	2.102

*Total iron as FeO. Calculated according to equation (tril) of Tischendorf et al. (1997). mgli, Mg-Li; feal, Fe + Mn + Ti - Al^{VI}; c, core; r, rim

average), locally in large xenomorphic crystals (up to 7 mm) and K-feldspar is mainly anhedral orthoclase (2 mm on average). It is kaolinitized and contains plagioclase and fluorite; perthite and microcline are almost absent. Plagioclase has an average size of 2 mm; it is sub-automorphic and most often altered. Dark mica (1 mm on average) is scarce and altered by chlorite. Secondary white mica is frequent; it develops at the expense of feldspar (up to 0.7 mm). Rare cubic zircon is included in mica and quartz (0.03 mm on average).

The *greisen* is closely associated with the two-mica granites. They are muscovite (0.3–3 mm) and quartz rich (3 mm on

average), K-feldspar free, and contain accessory fluorite (up to 0.7 mm) and allanite (up to 0.2 mm) (Fig. 5h).

Mineralogy

Analytical method

Major elements in feldspars and micas (Tables 1, 2, and 3) were determined by electron microprobe using a CAMECA-SX100 at the Microsonde Sud facility (Montpellier, France),

Table 3 Selected electron-microprobe analyses of dioctahedral micas (analyze in wt%) from Torak granitoids

Facies	Two-mica granite						Biotite granite			Alaskite
Sample	TA 15		TA 18				TA 29		TA 04	
Analyze N°	22	27	2	7	11	15	32	7 c	11	58
SiO ₂	46.46	45.19	44.69	46.14	44.95	45.73	47.79	47.46	48.04	47.71
TiO ₂	0.17	0.32	0.37	0.12	0.23	0.17	0.08	0.04	0.18	0.13
Al ₂ O ₃	29.61	29.86	29.77	27.23	29.86	29.12	30.50	31.74	27.24	30.63
FeO*	6.43	7.95	7.90	9.30	7.05	7.60	6.97	6.10	9.57	7.26
MnO	0.18	0.20	0.24	0.15	0.19	0.23	0.17	0.16	0.24	0.23
MgO	0.21	0.27	0.23	0.38	0.30	0.18	0.38	0.06	0.24	0.16
CaO	0.01	0.01	0.01	0.00	0.01	0.01	0.01	0.00	0.03	0.01
Na ₂ O	0.24	0.29	0.28	0.08	0.26	0.18	0.40	0.38	0.06	0.24
K ₂ O	11.03	10.90	10.76	10.89	10.88	10.67	10.56	9.86	9.49	10.48
Li ₂ O	1.00	0.92	0.49	1.24	0.82	0.85	1.39	0.54	0.93	0.20
F	2.02	1.89	1.18	2.37	1.74	1.78	2.59	1.28	1.92	0.60
Total	97.38	97.80	95.91	97.90	96.28	96.52	100.82	97.61	97.95	97.64
Structural formulae (on the basis of 22 oxygens)										
Si	6.361	6.215	6.229	6.400	6.243	6.339	6.331	6.360	6.560	6.416
Al ^{IV}	1.639	1.785	1.771	1.600	1.757	1.661	1.669	1.640	1.440	1.584
Al ^{VI}	3.140	3.055	3.120	2.853	3.133	3.097	3.093	3.374	2.945	3.270
Ti	0.018	0.034	0.039	0.012	0.024	0.018	0.008	0.004	0.019	0.013
Fe	0.736	0.915	0.921	1.079	0.818	0.880	0.772	0.683	1.093	0.817
Mn	0.021	0.023	0.028	0.017	0.022	0.027	0.019	0.018	0.028	0.026
Mg	0.044	0.056	0.047	0.080	0.062	0.037	0.074	0.011	0.048	0.032
Li	0.549	0.506	0.273	0.690	0.458	0.472	0.739	0.293	0.513	0.108
Ca	0.001	0.001	0.001	0.000	0.001	0.001	0.001	0.000	0.004	0.002
Na	0.064	0.076	0.075	0.023	0.069	0.049	0.102	0.098	0.016	0.063
K	1.927	1.913	1.912	1.928	1.928	1.887	1.785	1.685	1.654	1.798
F	0.873	0.822	0.518	1.041	0.765	0.782	1.083	0.541	0.829	0.254
OH	3.127	3.178	3.482	2.959	3.235	3.218	2.917	3.459	3.171	3.746
Sum cations	14.501	14.579	14.417	14.682	14.515	14.469	14.593	14.167	14.320	14.128
Fe/Fe + Mg	0.944	0.942	0.951	0.931	0.930	0.959	0.912	0.984	0.958	0.962
mgli	-0.506	-0.450	-0.226	-0.610	-0.397	-0.435	-0.665	-0.282	-0.465	-0.076
feal	-2.365	-2.084	-2.132	-1.745	-2.268	-2.172	-2.294	-2.669	-1.804	-2.415
Facies	Alaskite			Alkaline granite			Greisen			
Sample	TA 30		TA 16				TA 22			
Analyze N°	66	57	60	21	24	28	30	6	7	8
SiO ₂	48.43	47.60	47.98	48.10	46.66	46.56	48.24	48.05	48.00	48.45
TiO ₂	0.17	0.66	0.38	0.23	0.43	0.48	0.21	0.19	0.09	0.04
Al ₂ O ₃	32.28	27.53	26.33	30.68	30.60	30.88	30.46	30.56	32.20	30.68
FeO*	5.48	10.25	10.83	5.89	6.87	6.30	6.33	8.59	4.63	5.74
MnO	0.15	0.12	0.14	0.17	0.22	0.16	0.18	0.28	0.16	0.19
MgO	0.16	0.27	0.30	0.24	0.22	0.24	0.20	0.07	0.07	0.00
CaO	0.00	0.01	0.02	0.03	0.01	0.00	0.00	0.00	0.04	0.00
Na ₂ O	0.34	0.05	0.04	0.30	0.23	0.28	0.22	0.18	0.16	0.12
K ₂ O	10.97	10.97	10.89	9.21	9.71	9.15	9.58	11.12	11.00	11.21
Li ₂ O	0.20	0.01	0.10	1.10	0.75	0.83	0.27	0.71	0.67	0.81
F	0.60	0.07	0.34	2.17	1.63	1.75	0.75	1.57	1.49	1.49
Total	98.77	97.54	97.35	98.11	97.32	96.63	96.44	101.32	98.51	98.58
										98.90

Table 3 (continued)

Facies	Two-mica granite						Biotite granite				Alaskite	
Sample	TA 15		TA 18				TA 29		TA 04		TA 30	
Structural formulae (on the basis of 22 oxygens)												
Si	6.385	6.503	6.602	6.428	6.326	6.324	6.500	6.337	6.368	6.469	6.180	6.409
Al	1.615	1.497	1.398	1.572	1.674	1.676	1.500	1.663	1.632	1.531	1.820	1.591
Al ^{VI}	3.402	2.937	2.872	3.261	3.218	3.268	3.339	3.088	3.403	3.298	3.208	3.308
Ti	0.017	0.068	0.039	0.023	0.043	0.049	0.021	0.019	0.009	0.004	0.009	0.003
Fe	0.604	1.172	1.246	0.659	0.779	0.715	0.714	0.948	0.514	0.641	0.722	0.719
Mn	0.016	0.014	0.016	0.019	0.025	0.019	0.021	0.031	0.018	0.021	0.021	0.021
Mg	0.031	0.055	0.061	0.048	0.044	0.048	0.040	0.014	0.015	0.000	0.023	0.002
Li	0.107	0.006	0.053	0.590	0.409	0.451	0.145	0.421	0.380	0.358	0.432	0.288
Ca	0.000	0.001	0.002	0.004	0.002	0.000	0.000	0.000	0.006	0.000	0.000	0.000
Na	0.086	0.012	0.011	0.079	0.061	0.075	0.057	0.046	0.042	0.031	0.053	0.041
K	1.845	1.911	1.911	1.570	1.680	1.586	1.646	1.871	1.861	1.909	1.874	1.842
F	0.252	0.030	0.150	0.916	0.698	0.752	0.319	0.708	0.657	0.629	0.724	0.533
OH	3.748	3.970	3.850	3.084	3.302	3.248	3.681	3.292	3.343	3.371	3.276	3.467
Sum cations	14.109	14.177	14.212	14.252	14.260	14.211	13.984	14.437	14.247	14.262	14.343	14.224
Fe/Fe + Mg	0.951	0.955	0.954	0.932	0.947	0.937	0.947	0.985	0.972	1.000	0.969	0.998
mgli	-0.076	0.048	0.008	-0.541	-0.365	-0.403	-0.106	-0.407	-0.366	-0.358	-0.409	-0.286
feal	-2.765	-1.684	-1.571	-2.560	-2.371	-2.486	-2.582	-2.090	-2.863	-2.632	-2.457	-2.565

*Total iron as FeO. Calculated according to equation (di 1) of Tischendorf et al. (1997). mgli, Mg-Li; feal, Fe + Mn + Ti - Al^{VI}; c, core; r, rim

equipped with five wavelength-dispersive spectrometers. Operating conditions were 20-kV voltage, 10-nA current, and counting times of 20–30 s for peaks and background; standards were natural and synthetic minerals.

Results

Feldspars (Table 1) compositions are plotted in Or-Ab-An diagram (Fig. 6a). K-feldspar X_{Or} is 97% in biotite granite and 72 to 98% in alaskite. In biotite granite plagioclase is albite-oligoclase (An_{2–16}) and albite in the other facies (An_{1–8} in two-mica granite, An_{1–3} in alaskite and alkaline granite, and An_{1–2} in greisen).

Micas (Tables 2 and 3) are iron-rich ($0 \leq XMg \leq 0.09$; $XMg = Mg/(Mg + Fe^{2+})$), aluminous and fluorinated ($0.75 \text{ wt.\%} \leq F \leq 2.82 \text{ wt.\%}$), excepting for micas occurring in alaskite TA 30 (see Table 2) where four minerals were analyzed, which have fairly low fluorine contents with a mean of 0.36 wt.%. In the Al-M²⁺-Si diagram (Monier 1987) micas form two groups (Fig. 6b). The first group is defined by micas from the two-mica granite and biotite granite and plot close to the protholithionite pole ($3.39 < Al_{Tot} < 3.91$), while the micas from the other granite facies form the second group that plots between the zinnwaldite and trilithionite-muscovite poles

($4.27 < Al_{Tot} < 5.03$) indicating the presence of Li in the mica structure. In the mgli vs. feal plot [mgli = Mg-Li] and [feal = Fe^{tot} + Mn + Ti - Al^{VI}] classification diagram (Tischendorf et al. 1997, 1999) the mica analyses define also two groups (Fig. 6c). Trioctahedral mica is protholithionite ($F = 2.82 \text{ wt.\%}, Li_2O = 1.04 \text{ wt.\%}$) in two-mica granite, and ranges from siderophyllite (Fe micas) to protolithionite compositions (Li-Fe micas) ($0.87 \text{ wt.\%} < F < 2.66 \text{ wt.\%}, 0.80 \text{ wt.\%} < Li_2O < 1.13 \text{ wt.\%}$) in biotite granite (Fig. 6c, Table 2). Li contents increase in favor of the M²⁺ component in the siderophyllite-protolithionite direction. Dioctahedral mica from different Torak facies shows a weak evolution in composition similar to that for the trioctahedral mica (Fig. 6c, Table 3). The trend is initiated by weak Li and Fe compositions (phengite) to richer contents (Li-phengite) ($0.27 \text{ wt.\%} < Li_2O < 0.74 \text{ wt.\%}$) ($4.63 \text{ wt.\%} < FeO^* < 9.30 \text{ wt.\%}$). The more evolved alaskite TA 30 contain FeO-rich mica ($5.48 \text{ wt.\%} < FeO^* < 10.43 \text{ wt.\%}$) with poor Li and F contents ($0.01 \text{ wt.\%} < Li_2O < 0.2 \text{ wt.\%}, 0.07 \text{ wt.\%} < F < 0.6 \text{ wt.\%}$) and have phengite compositions.

Biotite compositions in both biotite granite and two-mica granite, are reported on the Al^{Tot}-Mg plot (Nachit et al. 1985) showing an Al^{Tot} content between 3.39 and 3.92. They initiate in this massif the alumino-potassic line represented by the lithic mica of the Tamanrasset-Taourirt group (Fig. 6d). All

Table 4 Major (wt%), trace (ppm) elements and CIPW-normative compositions for Torak studied rocks

Faciès	Two-mica granite		Biotite granite				Alaskite	Alkaline granite	Greisen
Sample Location	TA15 South Torak	TA18 South Torak	TA29 North Torak	TA31 North Torak	TA32	TA04 South Torak	TA30 North Torak	TA16 South Torak	TA22 South Torak
SiO ₂	75.49	75.52	75.87	73.95	75.95	76.86	74.23	75.94	75.25
TiO ₂	0.07	0.07	0.13	0.08	0.10	0.03	0.05	0.04	0.07
Al ₂ O ₃	12.41	12.55	12.55	12.55	12.20	12.44	13.34	12.46	13.03
Fe ₂ O ₃ t	1.16	1.59	1.70	1.44	1.59	1.12	0.84	0.82	2.28
MnO	0.02	0.02	0.03	0.03	0.03	0.02	0.01	0.02	0.07
MgO	0.07	0.07	0.07	0.07	0.07	0.000	0.07	0.06	0.07
CaO	0.68	0.94	0.91	0.31	0.92	0.23	0.77	0.23	0.71
Na ₂ O	3.47	3.08	3.16	2.87	3.17	3.27	3.11	3.64	1.90
K ₂ O	4.28	4.61	4.64	5.69	4.53	4.88	6.44	4.21	3.42
P ₂ O ₅	0.03	0.03	0.03	0.02	0.02	0.03	0.02	0.02	0.02
LOI	0.86	1.10	0.70	0.67	0.82	0.59	0.66	0.67	1.92
Total	98.54	99.57	99.78	97.68	99.40	99.46	99.55	98.10	98.74
Trace elements									
Be	4.162	3.791	3.855	3.632			7.853	6.959	
Ba	52.486	48.500	60.593	95.150			27.668	23.207	
Rb	610.382	617.053	608.969	634.345			781.645	497.960	
Sr	11.064	17.827	16.688	15.043	*18	*6	12.823	8.225	*13
Th	53.770	63.598	70.053	55.454			29.970	29.720	
U	11.582	17.661	11.518	19.792			11.337	8.931	
Zr *	119	149	156	125	161	79	56	64	62
Hf**	4.403	5.513	5.772	4.625	5.96	2.92	2.072	2.368	2.29
Nb	32.042	31.011	33.638	26.183			27.030	20.763	
Ta	3.975	4.480	3.803	2.474			3.766	2.914	
Y	141.446	175.955	167.761	111.132			174.578	76.739	
La	27.818	32.934	45.267	35.511			9.774	19.127	
Ce	72.686	76.834	110.951	82.412			23.508	48.732	
Pr	9.118	9.777	13.618	10.415			3.360	6.049	
Nd	36.279	38.888	51.549	40.517			14.562	23.538	
Sm	12.899	13.396	15.666	12.606			7.203	8.432	
Eu	0.158	0.193	0.241	0.287			0.105	0.079	
Gd	15.384	16.696	17.736	14.626			10.989	9.350	
Tb	3.110	3.256	3.373	2.572			2.558	2.016	
Dy	21.817	24.995	25.222	18.278			21.682	15.503	
Ho	4.612	5.591	5.390	3.707			4.957	3.414	
Er	14.927	17.878	17.199	10.482			16.753	11.026	
Tm	2.688	2.976	2.741	1.566			2.816	1.964	
Yb	18.860	20.604	18.543	9.926			20.888	13.473	
Lu	2.690	2.790	2.577	1.285			2.781	1.798	
Cr	26.000	< 20	< 20	< 20	< 20	< 20	< 20	37	< 20
Ni	35	38	38	30	42	23	37	24	36
LaN/YbN	0.997	1.080	1.650	2.418	—	—	0.316	0.959	—
HoN/YbN	0.713	0.791	0.847	1.088	—	—	0.692	0.738	—
DyN/LuN	0.811	0.896	0.979	1.423	—	—	0.780	0.862	—
Eu/Eu*	0.034	0.039	0.044	0.064	—	—	0.036	0.027	—
SumREE	243.05	266.81	330.07	244.19	—	—	141.94	164.50	—
CIPW norm									

Table 4 (continued)

Faciès	Two-mica granite		Biotite granite				Alaskite	Alkaline granite	Greisen
Sample Location	TA15 South Torak	TA18 South Torak	TA29 North Torak	TA31 North Torak	TA32	TA04 South Torak	TA30 North Torak	TA16 South Torak	TA22 South Torak
Fe ³⁺ /Total Fe as Fe ₂ O ₃	0.35	0.35	0.35	0.35	0.35	0.35	0.35	0.35	0.35
Quartz	37.93	38.01	37.59	35.34	38.16	38.81	29.93	38.87	50.39
Plagioclase	33.36	31.01	31.39	26.51	31.79	28.97	30.09	32.62	20.15
(Albite)	30.08	26.46	27.00	25.06	27.27	28.01	26.62	31.59	16.66
(Anorthite)	3.28	4.55	4.39	1.45	4.52	0.95	3.47	1.03	3.50
Orthoclase	25.95	27.71	27.72	34.75	27.20	29.20	38.50	25.57	20.93
Corundum	0.91	0.87	0.75	1.18	0.45	1.44	0.00	1.59	5.13
Diopsid	0.00	0.00	0.00	0.00	0.00	0.00	0.25	0.00	0.00
Hypersthene	1.02	1.36	1.35	1.26	1.32	0.87	0.65	0.78	2.02
Ilmenite	0.14	0.13	0.25	0.16	0.19	0.06	0.10	0.08	0.13
Magnetite	0.59	0.81	0.86	0.74	0.81	0.57	0.43	0.42	1.18
Apatite	0.07	0.07	0.07	0.05	0.05	0.07	0.05	0.05	0.05
Zircon	0.02	0.03	0.03	0.03	0.03	0.02	0.01	0.01	0.01
Total	100.00	100.00	100.00	100.00	100.00	100.00	100.00	100.00	100.00
DI	97.24	96.73	96.69	96.59	97.16	96.97	98.52	97.06	91.47
ASI	1.13	1.15	1.14	1.12	1.11	1.14	1.04	1.16	1.74
PI	1.60	1.63	1.61	1.47	1.58	1.53	1.40	1.59	2.45
Ag Ind	0.83	0.80	0.81	0.87	0.83	0.86	0.91	0.85	0.52

DI = CIPW-normative (quartz + orthoclase + albite + nepheline). ASI = A/CNK = Al/(Na + K + 2*(Ca - 3.3*P)) (atoms). PI = NK/A = (Na + K)/Al (atoms). Ag Ind = (Na + K)/Al (atoms). * = content measured by the XRF method. **Hf values were calculated from Zr using the Zr/Hf ratio of carbonaceous chondrite (McDonough and Sun 1995)

the studied biotites plot in the same line of peraluminous granitoids (Abdel-Rahman 1994) (Fig. 6e).

Major and trace element geochemistry

Analytical method

Based on the petrographic study, representative samples of the different petrographic types were selected for geochemical analysis (nine for major elements and six for trace elements) (Table 4). The samples were cut into small slabs to remove the thin traces of veins. Sample powders were obtained by crushing rock slabs in a jaw crusher and powdering fragments in an agate ring mill. Bulk rock major elements and minor elements (Cr, Ni, Sr, and Zr) were analyzed by X-ray fluorescence (XRF) at the Instituto Andaluz de Ciencias de la Tierra (IACT, Granada, Spain) using a Bruker AXS S4 Pioneer equipped with three analyzers (LiF200, OVO-55, PET). Within-run precision (% RSD), measured by repeated analyses of USGS reference materials as external standards, was better than 1.5% for all elements except P (2.7%). Bulk rock trace elements (REEs, Be, Sc, Sb, Cs, Rb, Ba, Th, U, Nb, Ta, Y, and Sc) were analyzed in solution using an Agilent 8800 QQQ

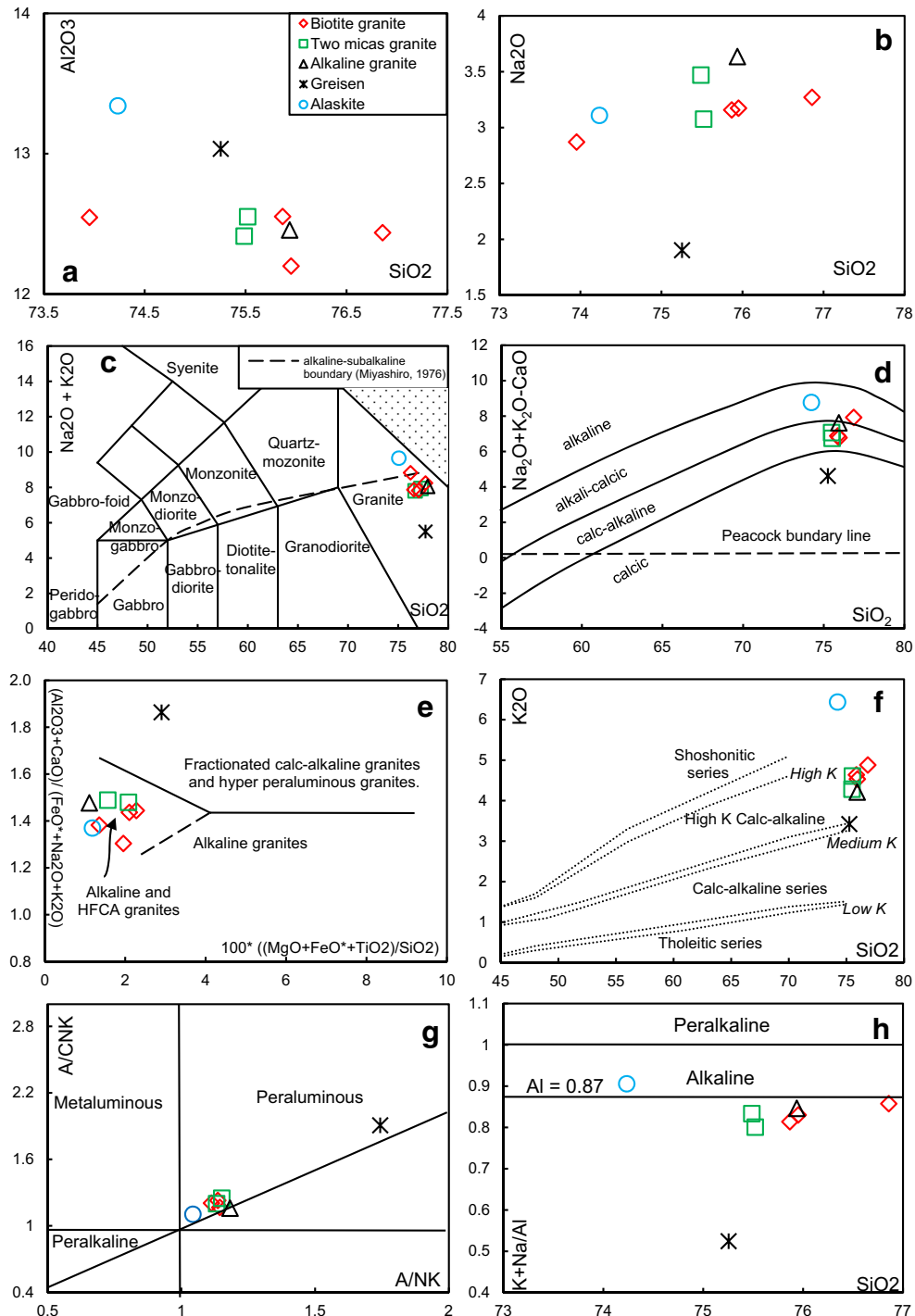
inductively coupled plasma mass spectrometer (ICP-MS) at IACT (Granada, Spain). Sample digestion was performed following the HF/HClO₄ dissolution and analytical procedure described in detail by Ionov et al. (1992) and Garrido et al. (2000). Bulk rock trace element concentrations were determined by external calibration, except for Hf that was calculated using Zr measured by XRF and the chondritic Zr/Hf ratio. Accuracy of the ICP-MS analyses was assessed from the results obtained for the international rock standards GS-N and AC-E, analyzed as an unknown during the same analytical runs as the Torak granitic samples.

Results

The studied rocks are all fresh except of greisen TA 22. The LOI contents vary between 0.86 wt.% and 1.1 wt.% for the two-mica granite, 0.59 wt.% and 0.82 wt.% for the biotite granites, and 0.67 wt.% for the alaskite and alkaline granite while the greisen reaches 1.92 wt.%, which confirms the results established on the petrographic and mineralogical criteria.

The contents of the different oxides show little variations from one granitic facies to another. Despite their great homogeneity in major elements, we can note in detail some

Fig. 7 Bulk rock major-element chemistry of the different granite facies of the Torak massif. **a** wt.% Al_2O_3 versus wt.% SiO_2 . **b** wt.% Na_2O versus wt.% SiO_2 . **c** TAS (total alkalis versus silica) diagram (Le Bas et al. 1986, 1992). **d** MALI (Modified Alkali Lime Index) diagram ($(\text{Na}_2\text{O} + \text{K}_2\text{O})/\text{CaO}$ vs. wt.% SiO_2) (Frost et al. 2001). **e** $100^*((\text{MgO} + \text{FeO} + \text{TiO}_2)/\text{SiO}_2)$ versus $(\text{Al}_2\text{O}_3 + \text{CaO})/(\text{FeO} + \text{Na}_2\text{O} + \text{K}_2\text{O})$ diagram separating calc-alkaline and alkaline granitoids with a third common field for alkaline granitoids and highly fractionated calc-alkaline (HFCA) granitoids (Sylvester 1998). **f** wt.% SiO_2 versus wt.% K_2O (subdivisions from Rickwood 1989). **g** Inverse agpaitic index A/NK (molar $\text{Al}/\text{Na} + \text{K}$) versus peraluminous index A/CNK (molar $\text{Al}/\text{Ca} + \text{Na} + \text{K}$) (Shand 1951). **h** Agpaitic index A.I (molar $(\text{K} + \text{Na})/\text{Al}$) vs. wt.% SiO_2 (Liégeois et al. 1998). The line at 0.87 separates the alkaline granitoids (above) from the sub-alkaline granitoids (Liégeois and Black 1987)



differences. The sum of the alkalis is most often equal to 8 wt.% but it reaches 9.5 wt.% in the alaskite TA 30 and does not exceed 5.3 wt.% in the greisen. The alaskite is distinguished by its high $\text{K}_2\text{O}/\text{Na}_2\text{O}$ ratio of 2.07 while in the other three facies this ratio is about 1.46 and 1.8 in the greisen (low Na_2O and K_2O). Al_2O_3 decreases slightly during the crystallization (Fig. 7a) while the sodium content, increases progressively in the course of the evolution emphasizing the role of

plagioclase (albite) during the crystallization (Fig. 7b). In fact, the Torak massif represents the liquid at the end of crystallization (group GII b granites; Azzouni-Sekkal and Boissonnas 1993) of the Taessa-Torak complex (see Fig. 2a). Alaskite shows the highest aluminum content ($\text{Al}_2\text{O}_3 = 13.34$ wt.%); however, its abnormal position in the studied rocks is probably due to leaching of the silica. Indeed, in many “Taourit” complexes (Azzouni-Sekkal 1989; Azzouni-Sekkal et al.

2003), the alaskite represents the liquid at the end of crystallization, with the highest SiO₂ contents, contrary to what appears in Fig. 7 a and b.

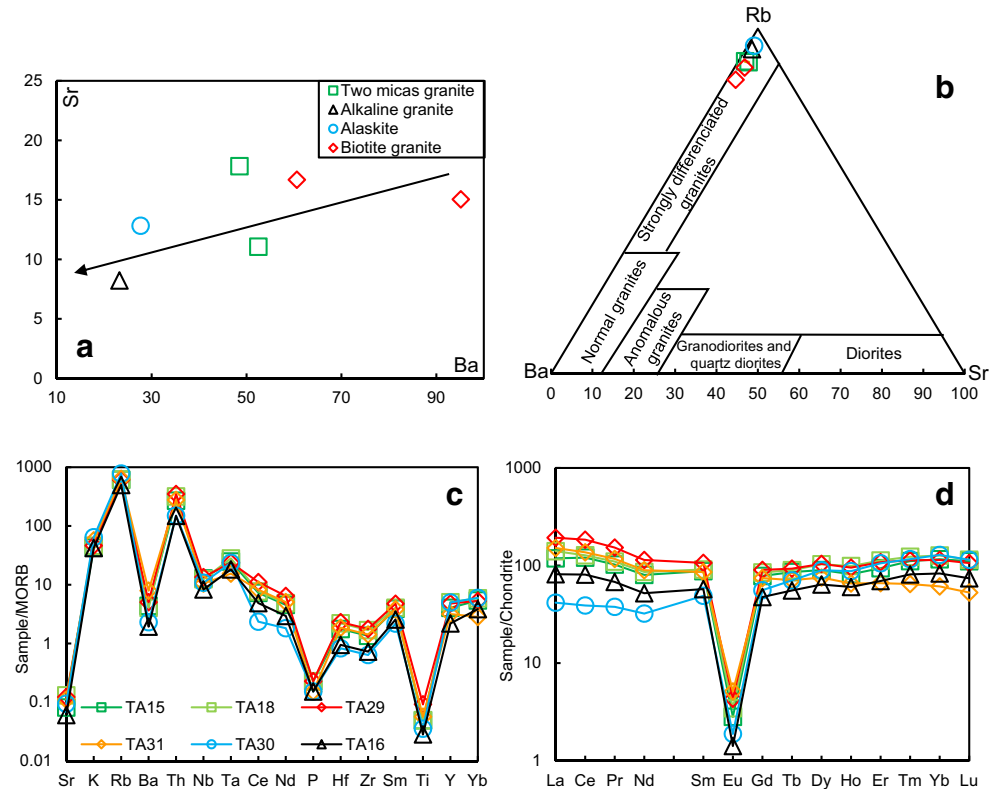
In the TAS diagram (Fig. 7c), only alaskite plots above the sub-alkaline-alkaline boundary. The calculated norm CIPW [calculated using Kurt Hollocher's CIPW Norm Excel program (http://minerva.union.edu/holloch/c_petrology/index.html) (Table 4)] indicates that all the Torak pluton facies contain normative corundum; they are therefore peraluminous, with the exception of the alaskite Ta 30; this confirms the alkaline character of this rock. The contents of orthoclase and albite are very close, the alaskite and greisen individualized here also by their higher normative orthoclase content than the albite. The MALI diagram (Frost et al. 2001) (Fig. 7d) indicates that the Torak granites belong to alkali-calcic series, typical of the post-collisional circular plutons of the Tuareg shield whereas the greisen plots in the calcic field. On the other hand, based on the criteria of Sylvester (1998) (Fig. 7e), the Torak granites are located in the common field of the high-fractionated calk-alkaline granites (HFCA). The enrichment in K₂O as indicated in the diagram of Rickwood (1989) (Fig. 7f) allows the Torak massif to be associated with high potassium calk-alkaline (HKCA) or even shoshonitic magmatism, well known during the late stage of the Pan-African orogeny in the Tuareg shield and especially the Hoggar. The Torak granites are peraluminous (A/CNK > 1) (Fig. 7g). In the agpaitic index AI versus SiO₂ diagram (Fig.

7 h) (Liégeois and Black 1987), all rocks are HKCA granites (AI < 0.87). Alaskite TA 30 displays high AI values (AI = 0.91) and projects into the alkaline series field (Fig. 7 h).

Regarding the trace elements compositions, Rb contents remain relatively high and constant (500 ppm < Rb < 780 ppm). In the diagram reported in Fig. 8a, Ba (23 ppm < Ba < 95 ppm) and Sr (8 ppm < Sr < 18 ppm) show a linear correlation for the entire sample population, highlighting the evolution of the series, from biotite granite to alkaline granite and alaskite, and the fractionation of feldspars. The Torak granites plot in the field of highly differentiated (alkaline) granites (EL Bouseily and El Sokkary 1975) (Fig. 8b).

The MORB-normalized diagrams (Fig. 8c) show the same patterns as the Silet-Taourirt GIIB and Laouni-Taourirt Baouinet subgroups (Azzouni-Sekkal and Boissonnas 1993, Azzouni-Sekkal et al. 2003). The positive anomalies in Rb, Th, Sm, and Y and to a lesser degree Ta and negative anomalies in Sr, Ba, P, and Ti and to a lesser degree, Nb highlight the fractionation of plagioclases, alkaline feldspars, apatite, ilmenite and/or titanite. The light depletion of Zr and Hf is linked to the enrichment of Th and Y by isomorphic substitution allowing crystallization of thorite, xenotime and monazite accessory minerals in the studied rocks. The Eu/Eu * ratio is less than 1 and is low due to plagioclase fractionation. The (La/Sm)N and (La/Yb)N ratios are very low and ≤ 2, which shows that the rare earths are not fractionated. The Torak REE patterns (Fig. 8d) show little or no fractionation and deep

Fig. 8 Trace elements variations for Torak pluton granites. **a** ppm Sr versus ppm Ba; **b** ppm Ba-Sr-Rb diagram (El Bouseily et al., 1975). **c** MORB-normalized incompatible element diagram. MORB values from Sun and McDonough (1989). **d** Chondrite-normalized REE patterns. Chondrite values from Sun and McDonough (1989)



negative Eu anomalies. This corresponds to tetrad effects on La–Ce–Pr–Nd and Gd–Tb–Dy–Ho suites of lanthanide elements (Bau 1996) resulting in gull wing-shaped patterns with downward concavity as all GIIb Taourirt groups (alaskite and alkali feldspars granite in Silet-Taourirt, Tamanrasset-Taourirt, and Laouni-Taourirts, Azzouni-Sekkal et al. 2003).

The use Ta vs Yb diagram (Pearce et al. 1984, Pearce 1996) (Fig. 9a) indicates that the studied granites have compositions of within-plate granite (WPG). Torak granites belong to the post-orogenic granites field on the Al_2O_3 vs. SiO_2 plot (Maniar and Piccoli 1989) (Fig. 9b). In the $(\text{Na}_2\text{O} + \text{K}_2\text{O})/\text{CaO}$ vs $(\text{Zr} + \text{Nb} + \text{Ce} + \text{Y})$ (Whalen et al. 1987), Torak granite project at the limit between the A-type granite field, and the fields of highly fractionated granites (Fig. 9c). On the other hand, they project into the field of A-type granites in the $(\text{FeO}_{\text{tot}}/\text{MgO})$ vs $(\text{Zr} + \text{Nb} + \text{Ce} + \text{Y})$ (Whalen et al. 1987)

Fig. 9 a ppm Ta versus ppm Yb (Pearce et al. 1984, Pearce 1996). b wt.% Al_2O_3 versus wt.% SiO_2 diagram (Maniar and Piccoli 1989) (IAG: island arc granitoids. CAG: continental arc granitoids; CCG: continental collision granitoids; POG: post-orogenic granitoids; RRG: rift-related granitoids; CEUG: continental epeirogenic uplift granitoids). c $(\text{Na}_2\text{O} + \text{K}_2\text{O})/\text{CaO}$ versus ppm Zr + Nb + Ce + Y diagram (Whalen et al., 1987). d % $\text{FeO}_{\text{tot}}/\text{MgO}$ versus Zr + Nb + Ce + Y (Whalen et al., 1987). e ppm Y-Nb-Ce diagram (Eby 1992) (Anorogenic A1-type granites relate to sources that are similar to ocean island basalt, evolving through partial melting or fractional crystallization; Anorogenic A2-type granites relate to sources that are like arc-type sources or average continental crust. A2-type granites derive by partial melting processes)

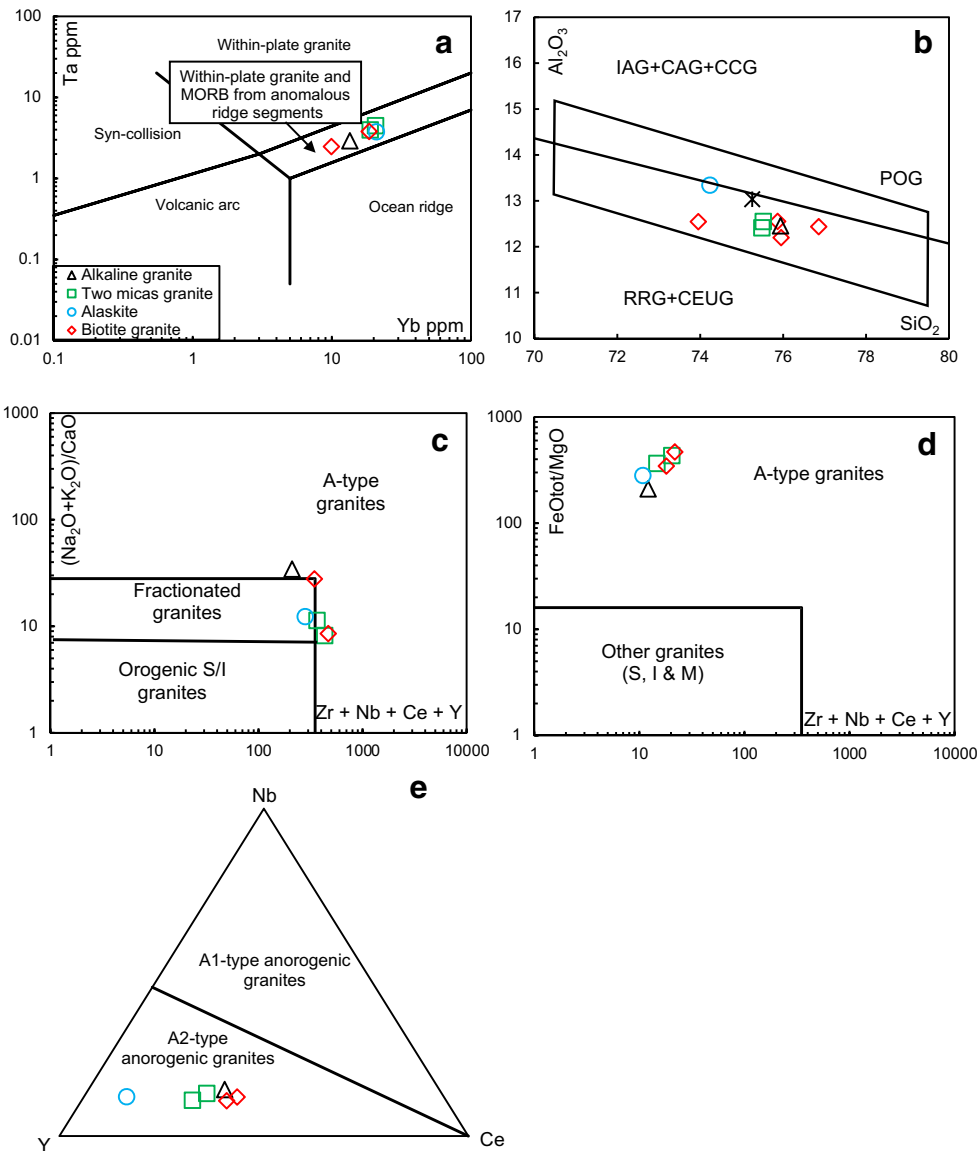


(Fig. 9d). In the ternary plot (Y, Nb, and Ce) (Eby 1992) (Fig. 9e), Torak granite project in the A2 granitoid group. The A2 group is generated in post-collisional or post-orogenic environments with significant crustal contribution.

Comparison with other Taourirt complexes from Tamanrasset and Laouni regions

The Torak pluton belongs to the Tamanrasset-Taourirt group (Azzouni-Sekkal et al. 2003). In this area, the GIIb Taourirt granites are widely spread. The Laouni-Taourirts and the Tamanrasset-Taourirts intruded the LATEA metacraton. The Laouni-Taourirts are undeformed and comprise the two complexes Baouinet North and Baouinet South emplaced within the Laouni terrane east of the $4^{\circ}50'$ E shear zone (Zaimen

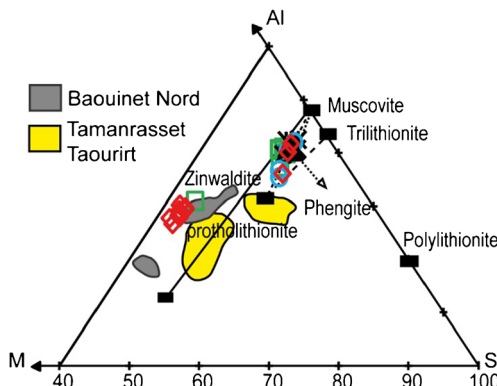


Fig. 10 Micas compositions from Torak granites, Tamanrasset-Taourirt, and Laouni-Taourirt reported in the $M^{2+} = (Fe + Mn + Mg)$ -Al-Si diagram (Monier 1987)

1994). The Tamanrasset-Taourirts include large massifs such as In Tounine, Ahele heg or smaller one such as Tessibent but also very small massifs made up of albite-topaz mineralized granites (Cheilletz et al. 1992; Ahmed-Said et al. 1995; Chalal and Marignac 1997; Kesraoui and Nedjari 2002) corresponding to the most evolved end-members of the Taourirt suite that were emplaced close to the boundary between Laouni and Azrou-n-Fad terranes.

The Torak granites and GIIb Taourirt granites show the same mineralogical compositions, mostly evidenced by the lack of amphibole and the occurrence of Li-micas and fluorite. Topaz is absent in the studied Torak granites. However, we cannot completely exclude its occurrence in the Torak pluton, considering its occurrence reported by Boissonnas (1974).

Studied micas of Torak compared to both Tamanrasset-Taourirt (In Tounine, Ahele heg, and albite-topaz mineralized granites) (Bouabsa 1987) and Laouni-Taourirt (Baouinet Nord) (Zaimen 1994) show similar composition with the two groups (Fig. 10). The Torak micas compositions show the lack of the phlogopite and are plotted midway between annite and sideropyllite poles ($0.956 \leq XFe \leq 0.990$; $2.33 \leq Al^{IV} \leq 2.46$). The protholithionite has a similar composition to the Baouinet while the Torak shows a second group of composition between zinnwaldite and trilithionite-muscovite poles, which reflects the aluminum-potassium scheme initiated by the Tamanrasset-Taourirt micas.

Geochemically most of the granitoids have SiO_2 content above 70 wt.%. Torak granites show similar alkali contents between 8 and 9.5 wt.% to the Tamanrasset-Taourirt and the Laouni-Taourirt Baouinet North. Torak granites and the two groups granites are entirely peraluminous (Fig. 11a), all granitites fall in an area between $(CaO/Al_2O_3)_{mol} = 0$ and 0.25. The abundance of Sr is roughly correlated with the Eu/Eu* ratio (Fig. 11b). The Torak granites and the Laouni-Taourirt Baouinet North are both characterized by a very low Sr and Eu/Eu*. This indicates a clear role of feldspar in the differentiation of the Taourirt granitoids. Comparing trace elements of different magmatic suites shows that the

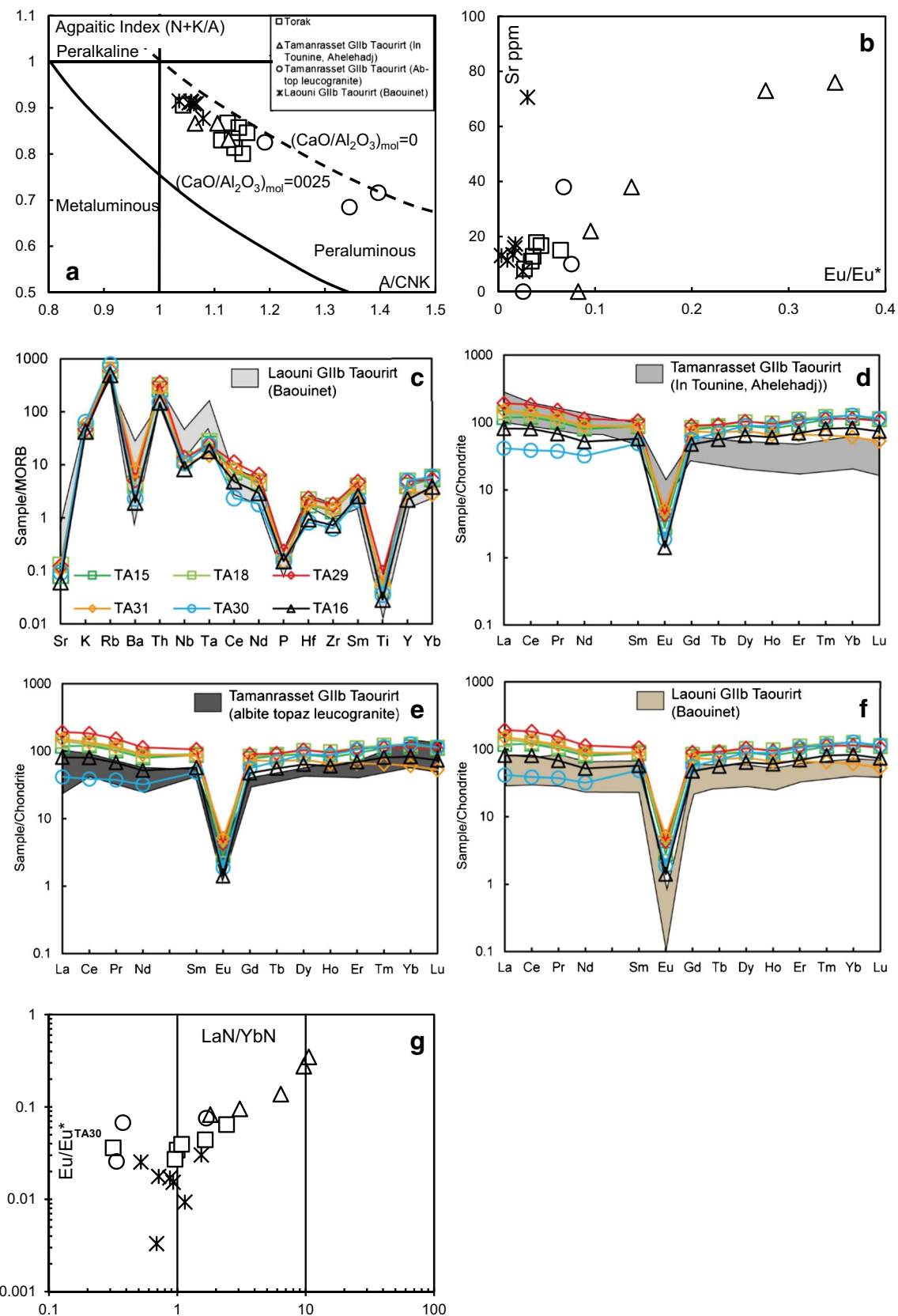
Fig. 11 Major and trace elements variations of the Torak granites compared with the Laouni and Tamanrasset-Taourirt groups granites. Data for Baouinet North granites (Laouni) form Zaimen (1994) and from Bouabsa (1987) for Tamanrasset-Taourirt granites. **a** A/CNK [$Al_2O_3/(CaO + Na_2O + K_2O)$ in molar proportion] versus agpaitic index [$(Na_2O + K_2O)/Al_2O_3$, in molar proportion] (Azzouni et al. 2003). **b** Eu/Eu* versus Sr ppm variation diagram. **c** MORB-normalized incompatible element diagrams. MORB values from Sun and McDonough (1989) **d, e, and f** Chondrite-normalized REE patterns. Chondrite values from Sun and McDonough (1989). **g** La_N/Yb_N versus Eu/Eu* for the various compared granites

incompatible element patterns are parallel with the same positive and negative anomalies. The granites of North Baouinet are more enriched in Ta (Fig. 11c). The comparison with Tamanrasset-Taourirt is prevented because of the lack of complete data. Torak granites MORB-normalized REE patterns are close to the Tamanrasset-Taourirt topaz leucogranites and Laouni-Taourirt Baouinet Nord (Fig. 11d, e, and f). Baouinet Nord granites show stronger negative anomalies (Fig. 11f). These REE characteristics can be summarized in a diagram Eu/Eu* vs. La_N/Yb_N (Fig. 11 g). The Laouni-Taourirt Baouinet North pluton compositions are similar to the different facies of the Torak granite while the Tamanrasset-Taourirt topaz leucogranites are similar to the Torak alaskite.

Discussion and conclusion

Studied granites of the Torak massif are highly differentiated ($DI > 96$) (Table 04). On the classification diagram, these rocks are represented by granites and rich K-feldspars granites (alkaline granites). These granites can be related to the alkali-calcic to alkaline magmatic series such as those defined for the “Taourirts” complexes (GIIb) because of the marked similarity between incompatible element patterns (Fig. 11e, f) of these rocks with Baouinet Nord granites and Tamanrasset topaz leucogranites. The samples plot on the boundary of the metaluminous, peraluminous, and peralkaline fields ($A/CNK \approx 1.1$) and are highly fractionated calc-alkaline granites (HKCA). Li contents in mica, increase systematically with evolution (Fig. 6c, Tables 2 and 3) reflecting hydrothermal magmatic process causing a supply of volatile elements (Li) at the end of the crystallization. In addition, seagull wing-shaped REE patterns due to high REE mobility is caused by F- and Cl-rich hydrothermal fluids that give sometimes greisens.

Torak granites show high Fe-index (> 0.95), post-collisional granitic affinity, alkali-calcic to alkaline character, and high REE content with Eu-negative anomalies; this led us to classify them as A-type granites. The constancy of ratios Zr/Hf and Ho/Y (Fig. 12a, b) [$Ho/Y (0.033 \pm 0.01)$, $Zr/Hf (27.03)$] during the fractional crystallization suggests a single and homogeneous source for all of the Torak rocks or a



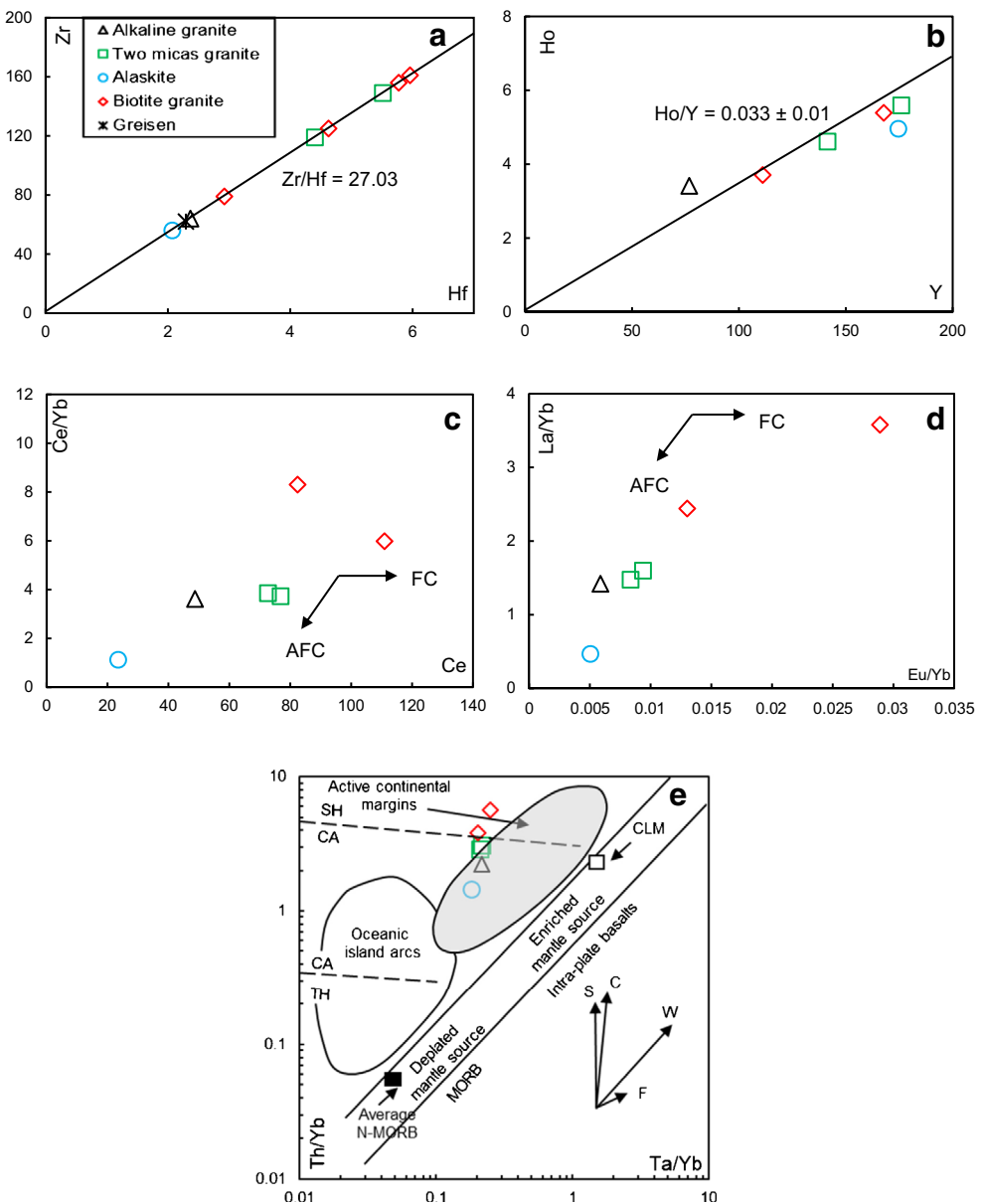
fractionating assemblage that do not modify these ratios (Sun and McDonough 1989).

The multi-element diagrams highlight the major role played by the continental crust in the genesis of the studied rocks (negative anomalies in Nb and Ti and positive in Th and Rb). The analyzed samples follow the AFC trend (Fig. 12c, d). Indeed the behavior of certain trace elements such as La, Ce, Yb, or Eu made it possible to highlight the contribution of the crust in the genesis of Torak rocks. Crustal contamination affects Th much more than Ta (Th is enriched in the continental crust) and the “crustal contamination” vector is sub-vertical (Pearce 1983) (Fig. 12e). The elements Th and Ta are therefore normalized with respect to the Yb in order to try to reduce the effect of partial melting or fractional crystallization and to better highlight the phenomenon of contamination. In this

diagram, the Torak granites (Fig. 12e) define a sub-vertical trend superimposable on that of crustal contamination, already mentioned by the trend of spiders. It is generally accepted that contamination mainly increases the concentrations of Th and Ba, which is the case of Torak granites. The analyzed samples plot between the calk-alkaline and shoshonitic domain (Fig. 12e) as already observed in the major elements, since they are highly fractionated calk-alkaline granites (HFCA).

It is currently admitted that the whole Taourit granites have the similar mixed deep source (asthenosphere+old lower crust) and that the most differentiated GIIB Taourit granites, have strongly interacted with their country rocks during emplacement (Azzouni-Sekkal et al. 2003). The Torak granites and in the light of the results of this study as well as the similarities they share with the most differentiated GIIB

Fig. 12 a ppm Zr versus Hf, b ppm Ho versus Y, c Ce/Yb versus ppm Ce, d La/Yb versus Eu/Yb diagrams. e Ta/Yb versus Th/Yb plot (Pearce, 1982, 1983). SCWF vectors indicating the influence of subduction components S., within plate enrichment W., crustal contamination C., and fractional crystallization F. Shoshonite/calc-alkaline SH/CA and calc-alkaline CA/TH series subdivisions are shown



Taourirt granites, could have the same source as these latter. The nature of their country rocks could correspond to the Eburnean (c. 2 Ga) gneiss of the Tefedest (LATEA). The trace elements analyses need to be implemented with isotopic data to better comprehend the nature of the contaminant and possibly the source of the Torak magmas.

The studied rocks may be related to the post-orogenic to anorogenic magmatism of the LATEA metacraton accompanied by a tectonic reactivation of the mega-shear zones with significant hydrothermal fluids circulation. This evolution is similar to that recently described in the Djanet terrane (570–540 Ma), which is caused by the collision between the Tuareg shield and the Murzukian craton (Fezaa et al. 2010). The situation of the Torak pluton and its NNW-SSE oriented structure could link its emplacement to the late Ediacaran intracontinental Murzukian orogenic phase that occurred in the eastern part of the Tuareg Shield.

References

- Abdallah N, Liégeois JP, Dewaele B, Fezaa N, Ouabadi A (2007) The Temaguessine Fe-cordierite orbicular granite (central Hoggar, Algeria): U-Pb SHRIMP age, petrology, origin and geodynamical consequences for the late Pan-African magmatism of the Tuareg shield. *J Afr Earth Sci* 49:153–178
- Abdel-Rahman AM (1994) Nature of biotites from alkaline, calc-alkaline, and peraluminous magmas. *J Petrol* 35:525–541
- Abdelsalam M, Liégeois JP, Stern RJ (2002) The Saharan metacraton. *J Afr Earth Sci* 34:119–136
- Acef K, Liégeois JP, Ouabadi A, Latouche L (2003) The Anfeg postcollisional pan-African high-K calc-alkaline batholith (Hoggar, Algeria), emplaced within the LATEA metacraton. *J Afr Earth Sci* 37:295–311
- Ahmed-Said Y, Leake BE, Bouabsa L, Moulahoum O (1995) The central Hoggar Taourirt and albite-topaz post Pan-African granites (southern Algeria); their petrology, geochemistry and petrogenesis. *Neues Jahrbuch für Mineralogie, Abhandlungen* 170: 21–57
- Azzouni-Sekkal A (1989) Pétrologie et géochimie des granites de type “Taourirt”: un exemple de province magmatique de transition entre les régimes orogéniques et anorogéniques, au Pan-Africain (Hoggar-Algérie). Thèse USTHB, Alger, 667 pp. and Mémoire Service Géologique Algérie, 1995, 7, Boumerdes, 288 pp.
- Azzouni-Sekkal A, Boissonnas J (1993) Une province magmatique de transition du calco-alkalin à l’alcalin : les granitoïdes panafricains à structure annulaire de la chaîne pharúsienne du Hoggar (Algérie). *Bulletin Soc Géol Fr* 164:597–608
- Azzouni-Sekkal A, Liégeois JP, Bechiri-Benmerzoug F, Belaïdi-Zinet S, Bonin B (2003) The “Taourirt” magmatic province, a marker of the closing stages of the pan-African orogeny in the Tuareg shield: review of the available data and Sr- Nd isotope evidence. *J Afr Earth Sci* 37:337–350
- Bau M (1996) Controls on the fractionation of isovalent trace elements in magmatic and aqueous systems. Evidence from Y/ho, Zr/Hf and lanthanide tetrad effect. *Contrib Mineral Petro* 123:323–333
- Bendaoud A, Ouzegane K, Godard G, Liégeois JP, Kienast JR, Bruguier O, Draren A (2008) Geochronology and metamorphic P-T-X evolution of the eburnean granulite-facies metapelites of Tidjenouine (central Hoggar, Algeria): witness of the LATEA metacratonic evolution. In: Ennih N, Liégeois JP (eds) The boundaries of the west African Craton, vol 297. Special Publication, Geological Society of London, pp 111–146
- Bertrand JML, Caby R, Ducrot J, Lancelot JR, Moussine-Pouchkine A, Saadallah A (1978) The late pan-African intracontinental linear fold belt of the U/Pb geochronology, tectonic implications for the Hoggar shield. *Precambrian research* 7: 349–376. Eastern Hoggar (Central Sahara, Algeria): geology, structural development, U/Pb geochronology, tectonic implications for the Hoggar shield. *Precambrian Res* 7:349–376
- Black R, Latouche L, Liégeois JP, Caby R, Bertrand JM (1994) Pan-African displaced terranes in the Tuareg shield (Central Sahara). *Geology* 22:641–664
- Boissonnas J (1974) Les granites à structures concentriques et quelques autres granites tardifs de la chaîne panafricaine (Sahara central, Algérie). Thèse, Centre de Recherche sur les zones Arides, Série Géologie 16: 662pp
- Bouabsa L (1987) Intrusions granitiques à albite-topaze: minéralisations stanno-wolframifère et altérations hydrothermales associées. L'exemple du Hoggar central. Thèse Université Nancy I, France, 193 pp.
- Chalal Y, Marignac C (1997) Découverte de wolframo-ixiolite dans les microgranites à albite-topaze d'Alameda (Hoggar central, Algérie) : implications métallogéniques. *Bull Serv Géol Algér* 8:71–79
- Cheilletz A, Bertrand JM, Charoy B, Moulahoum O, Bouabasa L, Farrar E, Zimmerman JL, Dautel D, Archibald DA, Boullier AM (1992) Géochimie et géochronologie Rb-Sr, K-Ar et 39Ar-40Ar des complexes granitiques panafricains de la région de Tamanrasset (Algérie) : relations avec les minéralisations Sn-W associées et l'évolution tectonique du Hoggar central. *Bull Soc Géol Fr* 163: 733–750
- Eby GN (1992) Chemical subdivision of the A-type granitoids: petrogenetic and tectonic implications. *Geology* 20:641–644
- EL Bouseily AM, El Sokkary AA (1975) The relation between Rb, Ba and Sr in granitic rocks. *Chem Geol* 16:207–219
- Fezaa N, Liégeois JP, Abdallah N, Cherfouh EH, De Waele B, Bruguier O, Ouabadi A (2010) Late Ediacaran geological evolution (575–555 ma) of the Djanet terrane, eastern Hoggar, Algeria, evidence for a Murzukian intracontinental episode. *Precambrian Res* 180:299–327
- Frost BR, Barnes C, Collins WJ, Arculus RJ, Ellis D, Frost CD (2001) A geochemical classification for granitic rocks. *J Petrol* 42:2033–2048
- Garrido CJ, Bodinier JL, Alard O (2000) Incompatible trace element partitioning and residence in anhydrous spinel peridotites and websterites from the Ronda orogenic peridotite. *Earth Planet Sci Lett* 181:341–358
- Ikhlef-Debabha F, Azzouni-Sekkal A, Benhallou AZ, Ben El Khaznadjji R, Dautria JM, Bonin B (2014) Premières données cartographiques sur l’association acide-basique (massif granitique de Taessa complexe mafique-ultramafique d’Edikel), terrane de Laouni (LATEA, Hoggar central, Algérie). Colloque national sur la géologie et les ressources minérales du Hoggar, Algeria pp 75–76
- Ionov DA, Savoyant L, Dupuy C (1992) Application of the ICP-MS technique to trace element analysis of peridotites and their minerals. *Geostand Geoanal Res* 16(2):311–315
- Kesraoui M, Nedjari S (2002) Contrasting evolution of low-P rare metal granites from two different terranes in the Hoggar area, Algeria. *J Afr Earth Sci* 34:247–257
- Le Bas MJ, Le Maitre RW, Streckeisen A, Zanettin B (1986) A chemical classification of volcanic rocks based on the total alkali e silica diagram. *J Petrol* 27:745–750
- Le Bas MJ, Le Maitre RW, Woolley AR (1992) The construction of the total alkali-silica chemical classification of volcanic rocks. *Mineral Petro* 46:1–22
- Liégeois JP (2019) A new synthetic geological map of the Tuareg shield: an over-view of its global structure and geological evolution. In: The geology of the Arab world—an overview. Springer, Cham, pp 83–107

- Liégeois JP, Abdelsalam MG, Ennih N, Ouabadi A (2013) Metacraton: nature, genesis and behavior. *Gondwana Res* 23:220–237
- Liégeois JP, Black R (1987) Alkaline magmatism subsequent to collision in the pan-African belt of the Adrar des Iforas. In: Fitton JG, Upton BGJ (eds) alkaline igneous rocks, vol 30. Geol Soc Lond Spec Publ, pp 381–401
- Liégeois JP, Latouche L, Bougrara M, Navez J, Guiraud M (2003) The LATEA metacraton (central Hoggar, Tuareg shield, Algeria): behaviour of an old passive margin during the pan-African orogeny. *J Afr Earth Sci* 37:161–190
- Liégeois JP, Navez J, Hertogen J, Black R (1998) Contrasting origin of postcollisional high-K calc-alkaline and shoshonitic versus alkaline and peralkaline granitoids. The use of sliding normalization. *Lithos* 45:1–28
- Maniar PD, Piccoli PM (1989) Tectonic discrimination of granitoids. *Geol Soc Am Bull* 100:65–643
- McDonough WF, Sun SS (1995) The composition of the earth. *Chem Geol* 120:223–253
- Monier G (1987) Cristallochimie de micas des leucogranites. Nouvelles données expérimentales et applications pétrologiques. *Géol Mém CREGU*, Nancy, 14: 347p
- Nachit H, Razafimahefa N, Stussi JM, Caron J (1985) Composition chimique des biotites et typologie magmatique des granitoïdes. *Comptes Rendus de l'Académie des Sciences, Paris* 301: 813–818
- Pearce JA (1983) The role of sub-continental lithosphere in magma genesis at destructive plate margins. In: Hawkesworth CJ, Norry MJ (eds) Continental basalts and mantle xenoliths. Shiva, Orpington, pp 230–249
- Pearce JA, Harris NBW, Tindle AG (1984) Trace element discrimination diagrams for the tectonic interpretation of granitic rocks. *J Petrol* 25: 956–983
- Pearce JA (1996) Sources and settings of granitic rocks. *Episodes* 19: 120–125
- Rickwood PC (1989) Boundary lines within petrologic diagrams, which use oxides of major and minor elements. *Lithos* 22:247–264
- Peucat JJ, Draren A, Latouche L, Deloule E, Vidal P (2003) U–Pb zircon (TIMS and SIMS) and Sm–Nd whole rock geochronology of the Gour Oumalelen granulitic basement, Hoggar massif, Tuareg shield, Algeria. *J Afr Earth Sci* 37:229–239
- Shand SJ (1951) Eruptive rocks: their genesis, composition, classification and their relation to ore-deposit with a chapter on meteorites, 4th edn. Wiley, New York, p 488
- Sun SS, McDonough WF (1989) Chemical and isotopic systematics of oceanic basalts: implications for mantle composition and processes. In: Saunders AD, Norry MJ (Ed), *Magmatism in the ocean basins*, 42. Geological society, London 313–345. Special Publication, 42, 313, 345
- Sylvester PJ (1998) Post-collisional strongly peraluminous granites. *Lithos* 45:29–44
- Tischendorf G, Gottesmann B, Förster HJ, Trumbull RB (1997) On Libearing micas: estimating Li from electron microprobe analyses and an improved diagram for graphical representation. *Mineral Mag* 6:809–834
- Tischendorf G, Förster HJ, Gottesmann B (1999) The correlation between lithium and magnesium in trioctahedral micas: improved equations for Li₂O estimation from MgO data, *Mineralogical Magazine* vol 63: 57–74
- Vitel G (1979) La région de Tefedest-Atakor du Hoggar central (Sahara). Evolution d'un complexe granulitique précambrien. These d'Etat, Paris VII 333 p
- Whalen JB, Currie KL, Chappell BW (1987) A-type granites: geochemical characteristics, discrimination and petrogenesis. *Contrib Mineral Petrol* 95:407–419
- Zaimen F (1994) Mise en évidence de plusieurs suites magmatiques dans la partie occidentale du terrain de Laouni (Hoggar, Algérie). Thèse Doctorat en Sciences, Université de Paris-Sud, Orsay, 175 p